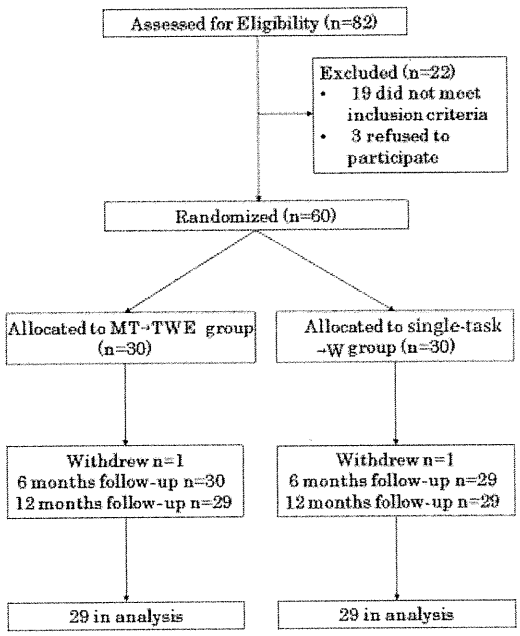

Figure 2. A flow chart showing the distribution of participants throughout the trial.

All 16 of the scheduled intervention session were completed. The median relative adherence was 100% (25th–75th percentile, 94–100%) for the TWE group and 100% (94%–100%) for the W group. No health problems, including cardiovascular or musculoskeletal complications, occurred during training sessions or testing. Minor problems observed in both groups included aching muscles after the first training sessions and fatigue. All problems were managed easily using adjustment of the intervention and improved during intervention.

Baseline Characteristics

Participants in the TWE and W groups were comparable and well matched with regard to their baseline characteristics. There were no significant differences between group means for age (TWE = 79.5 ± 6.2, W = 81.4 ± 4.9; P = .20), body weight (TWE = 52.3 ± 9.9 kg, W = 50.7 ± 7.1 kg; P = .47), height (TWE = 146.7 ± 7.3 cm, W = 146.6 ± 6.9 cm; P = .96), number of medications (TWE = 3.8 ± 2.8, W = 3.7 ± 2.9; P = .89), experiencing a fall within the past year (TWE = 37.9%, W = 34.5%; P = .50), or MMSE score (TWE = 27.8 ± 2.1 points, W = 28.0 ± 1.7 points; P = .79).

Effects of the Interventions on Fall Rate 6 and 12 Months After Trial Completion

Two participants (6.9%) in the TWE group and 10 (34.5%) in the W group had experienced a fall by 6 months after trial completion. During the 6-month follow-up period, the IRR of falls for the TWE group compared with the W group was 0.20 (95% CI = 0.04–0.91). Five participants (17.2%) in the TWE group and 11 (37.9%) in the W group had experienced a fall by 12 months after trial completion. During the 12-month follow-up period, the IRR of falls for the TWE group compared with the W group was 0.45 (95% CI = 0.16–1.77).

Effects of the Interventions on Secondary Outcome Measures 6 and 12 Months After Trial Completion

Participants in the TWE group had significantly greater improvements in secondary outcome measures including TWT, TUG, TMT, DT walking time, and DT walking step, although there were no significant group and time effects without the group × time interactions (Table 1). Post hoc Bonferroni tests showed significant differences in favor of the TWE group in several cases: TWT after the intervention and 6 months after the intervention, TMT after the intervention, and DT walking time 6 months after the intervention.

DISCUSSION

The TWE program is a multicomponent walking program that was designed to address multiple domains such as attention, short-term memory, and balance that, when impaired, have been shown to increase fall risk.[9] The multidirectional steps in the forward, backward, lateral, and oblique directions during TWE lead to better activation of synergistic and agonistic leg muscles. Therefore, it is possible that the TWE regimen improves many aspects of the functional fitness of the lower extremities.

The differences in fall rates between the TWE and W groups were significant 6 months after the intervention but not 12 months after the intervention. Balance, gait, and coordination have been practiced in many studies by performing isolated exercises. In contrast, in this trial, these physical tasks were practiced in an exercise environment that simulated complex situations. In this way, participants may also learn to recognize potentially hazardous situations and adopt strategies to minimize the risk of falling. The results of this trial show that the intervention resulted in functional changes related to locomotion skills under complex-task conditions. Several cognitive training programs have been shown to be effective at improving memory, reasoning, and speed of processing of older adults,[18,19] and previous work has shown that community-dwelling older adults living with a history of falling have significantly slower TMT times than nonfallers.[20] The training effect on TUG and DT walking, which are useful for evaluating the risk of falling,[13,16] were also better after the intervention in the TWE group. These results may indicate the importance of instructions when training under complex-task conditions and suggest that effectively improving these functions could lead to a decrease in fall rate. The maintenance periods of an improvement in physical function and that of fall prevention were the same 6 months after trial completion.

This trial has notable limitations. First, these findings should be seen as preliminary because of the small sample size. Second, the statistical analysis of each of the outcome measures, including the physical performance tests, cognitive tests, and fall rate, were performed separately, which increases the risk of false-positive findings. Third, participants in both groups were probably more motivated and showed greater interest in health issues and fall risk than the general population of older adults.

The results of this pilot RCT suggest that the TWE strategy was more effective in improving locomotion

Table 1. Fitness Items According to Group Before and After the Intervention

Item	Mean ± Standard Deviation				*F*-Value 1.Time Effect 2. Group × Time
	Before the Intervention	After the Intervention	6 Months After the Intervention	12 Months After the Intervention	
Trail-walking test, s					
TWE group	66.9 ± 15.4	54.1 ± 9.9†	61.0 ± 10.1†	67.1 ± 14.5	17.93**
W group	67.8 ± 10.1	70.2 ± 11.7‡	69.4 ± 11.4‡	69.9 ± 10.9	12.06**
Trail-Making Test, n					
TWE group	81.2 ± 47.6	63.6 ± 29.6†	67.2 ± 32.0†	80.3 ± 46.8	12.67**
W group	83.6 ± 39.3	82.1 ± 3.59‡	82.6 ± 33.7	84.3 ± 39.2	8.40**
Timed Up and Go Test, seconds					
TWE group	12.3 ± 2.6	11.0 ± 2.0†	11.5 ± 2.0	11.6 ± 2.6	5.97**
W group	12.4 ± 2.7	12.1 ± 2.4	12.8 ± 2.9	13.0 ± 3.4	2.98*
Functional reach, cm					
TWE group	24.9 ± 6.4	22.2 ± 5.9	25.3 ± 6.7	24.6 ± 6.4	1.62
W group	23.7 ± 6.1	24.3 ± 6.5	24.4 ± 4.8	24.7 ± 4.1	1.77
One-leg stand, seconds					
TWE group	6.4 ± 5.5	5.4 ± 4.8	6.7 ± 6.3	5.9 ± 4.9	0.49
W group	5.4 ± 5.0	4.8 ± 2.3	4.6 ± 5.4	5.2 ± 5.7	0.49
10-m walking time, seconds					
TWE group	11.5 ± 2.6	11.4 ± 2.2	11.5 ± 2.8	11.2 ± 2.9	0.57
W group	11.4 ± 3.0	11.5 ± 2.7	12.0 ± 2.9	12.5 ± 3.6	1.53
10-m walking time, steps					
TWE group	22.3 ± 4.1	22.7 ± 32	22.5 ± 3.8	22.3 ± 3.7	0.52
W group	22.8 ± 5.1	22.1 ± 4.8	22.8 ± 4.5	23.2 ± 4.7	1.46
Dual-task 10-m walking time, seconds					
TWE group	17.4 ± 6.5	14.9 ± 3.4†	15.9 ± 5.3‡	16.1 ± 5.3	2.48
W group	16.4 ± 3.7	16.3 ± 4.6	18.6 ± 3.6	18.2 ± 4.6	2.85*
Dual-task10-m walking step, steps					
TWE group	23.2 ± 3.5	22.6 ± 3.2	22.5 ± 3.4	22.6 ± 3.5	1.05
W group	22.6 ± 4.8	23.4 ± 5.8	24.3 ± 3.6	24.6 ± 4.6	2.67*

† As calculated by comparing preintervention values.
‡ As calculated by group comparison.
$P<$ **.01, *.05.
TWE = trail-walking exercise; W = walking.

and cognitive performance under complex-task conditions than walking only. In addition, participants who received individualized complex-task training combined with a traditional intervention demonstrated a lower incident rate of falls 6 months after trial completion. Further research is needed, but this preliminary result may lead to a new intervention for fall prevention.

ACKNOWLEDGMENTS

The authors wish to acknowledge Dr. Toshiro Sakata and Mr. Toshiaki Uehara for their major contribution to the data collection.

Conflict of Interest: This work was supported by grants from Kyoto University.

Author Contributions: All of the authors took significant role in every aspect of this study.

Sponsor's Role: None.

REFERENCES

1. Blake AJ, Morgan K, Bendall MJ et al. Falls by elderly people at home: Prevalence and associated factors. Age Ageing 1988;17:365–372.
2. Tinetti ME, Speechley M, Ginter SF. Risk factors for falls among elderly persons living in the community. N Engl J Med 1988;319:1701–1707.
3. Gillespie LD, Gillespie WJ, Robertson MC et al Interventions for preventing falls in elderly people. Cochrane Database Syst Rev 2009; (2): CD000340.
4. Robertson MC, Campbell AJ, Gardner MM et al. Preventing injuries in older people by preventing falls: A meta–analysis of individual–level data. J Am Geriatr Soc 2002;50:905–911.
5. Boulgarides LK, McGinty SM, Willett JA et al. Use of clinical and impairment–based tests to predict falls by community-dwelling older adults. Phys Ther 2003;83:328–339.
6. Woollacott M, Shumway-Cook A. Attention and the control of posture and gait: A review of an emerging area of research. Gait Posture 2002;16:1–14.
7. Shumway-Cook A, Woollacott M, Kerns KA et al. The effects of two types of cognitive tasks on postural stability in older adults with and without a history of falls. J Gerontol A Biol Sci Med Sci 1997;52A:M232–M240.
8. Shumway-Cook A, Guralnik JM, Phillips CL et al. Age–associated declines in complex walking task performance: The Walking InCHIANTI toolkit. J Am Geriatr Soc 2007;55:58–65.
9. Yamada M, Ichihashi N. Predicting the probability of falls in community-dwelling elderly individuals using the trail walking test (TWT). Environ Health Prev Med (in press).

10. Folstein MF, Folstein SE, McHugh PR. "Mini-mental state". A practical method for grading the cognitive state of patients for the clinician. J Psychiatr Res 1975;12:189–198.
11. Buchner DM, Cress ME, de Lateur BJ et al. The effect of strength and endurance training on gait, balance, fall risk, and health services use in community–living older adults. J Gerontol A Biol Sci Med Sci 1997;52A: M218–M224.
12. Koski K, Luukinen H, Laippala P et al. Physiological factors and medications as predictors of injurious falls by elderly people: A prospective population–based study. Age Ageing 1996;25:29–38.
13. Podsiadlo D, Richardson S. The timed "Up & Go": A test of basic functional mobility for frail elderly persons. J Am Geriatr Soc 1991;39:142–148.
14. Duncan PW, Studenski S, Chandler J et al. Functional reach: Predictive validity in a sample of elderly male veterans. J Gerontol 1992;47:M93–M98.
15. Lopopolo RB, Greco M, Sullivan D et al. Effect of therapeutic exercise on gait speed in community–dwelling elderly people: A meta–analysis. Phys Ther 2006;86:520–540.
16. Beauchet O, Dubost V, Allali G et al. 'Faster counting while walking' as a predictor of falls in older adults. Age Ageing 2007;36:418–423.
17. Army Individual Test Battery. Manual of Directions and Scoring. Washington, DC: War Department, Adjutant General's Office, 1944.
18. Ball K, Berch DB, Helmers KF et al. Effects of cognitive training interventions with older adults: A randomized controlled trial. JAMA 2002;13:2271–2281.
19. Edwards JD, Wadley VG, Vance DE et al. The impact of speed of processing training on cognitive and everyday performance. Aging Ment Health 2005;9:262–271.
20. Lord SR, Fitzpatrick RC. Choice stepping reaction time: A composite measure of falls risk in older people. J Gerontol A Biol Sci Med Sci 2001;56A:M627–M632.

THE JOURNAL OF BIOLOGICAL CHEMISTRY VOL. 285, NO. 39, pp. 29842–29850, September 24, 2010

Histone Modifiers, YY1 and p300, Regulate the Expression of Cartilage-specific Gene, Chondromodulin-I, in Mesenchymal Stem Cells*[S]

Received for publication, February 24, 2010, and in revised form, July 21, 2010 Published, JBC Papers in Press, July 27, 2010, DOI 10.1074/jbc.M110.116319

Tomoki Aoyama[‡§¶], Takeshi Okamoto[‡§], Kenichi Fukiage[‡§], Seiji Otsuka[‡‖], Moritoshi Furu[‡§], Kinya Ito[‡‖], Yonghui Jin[‡], Michiko Ueda[‡], Satoshi Nagayama[**], Tomitaka Nakayama[§], Takashi Nakamura[§], and Junya Toguchida[‡§‡‡1]

From the [‡]Institute for Frontier Medical Sciences, the [‡‡]Center for iPS Cell Research and Application, Kyoto University, Kyoto 606-8507, the [§]Department of Orthopaedic Surgery, [¶]Human Health Sciences, and the [**]Department of Surgery and Surgical Basic Science, Graduate School of Medicine, Kyoto University, Kyoto 606-8507, Japan and the [‖]Department of Musculoskeletal Medicine, Graduate School of Medical Sciences, Nagoya City University, Nagoya 467-8601, Japan

Elucidating the regulatory mechanism for tissue-specific gene expression is key to understanding the differentiation process. The chondromodulin-I gene (*ChM-I*) is a cartilage-specific gene, the expression of which is regulated by the transcription factor, Sp3. The binding of Sp3 to the core-promoter region is regulated by the methylation status of the Sp3-binding motif as we reported previously. In this study, we have investigated the molecular mechanisms of the down-regulation of *ChM-I* expression in mesenchymal stem cells (MSCs) and normal mesenchymal tissues other than cartilage. The core-promoter region of cells in bone and peripheral nerve tissues was hypermethylated, whereas the methylation status in cells of other tissues including MSCs did not differ from that in cells of cartilage, suggesting the presence of inhibitory mechanisms other than DNA methylation. We found that a transcriptional repressor, YY1, negatively regulated the expression of *ChM-I* by recruiting histone deacetylase and thus inducing the deacetylation of associated histones. As for a positive regulator, we found that a transcriptional co-activator, p300, bound to the core-promoter region with Sp3, inducing the acetylation of histone. Inhibition of YY1 in combination with forced expression of p300 and Sp3 restored the expression of *ChM-I* in cells with a hypomethylated promoter region, but not in cells with hypermethylation. These results suggested that the expression of tissue-specific genes is regulated in two steps; reversible down-regulation by transcriptional repressor complex and tight down-regulation via DNA methylation.

The expression of cell lineage-specific genes is a key to initiating the differentiation of stem cells into a particular cell lineage, and the down-regulation of such genes in cells of other lineages is also critical to maintain a normal cellular physiology. The chondromodulin-I (*ChM-I*)[2] gene is a specific gene for cartilage tissue (1). We have found that the basal promoter activity of *ChM-I* is driven by a ubiquitous transcription factor, Sp3, and chondrocyte-specific expression is regulated by the methylation status of the Sp3-binding motif in the core-promoter region (2). Demethylation treatment *in vitro* restored the expression of *ChM-I* in cells of the osteogenic lineage (2, 3). A similar result was obtained with cells of the adipogenic lineage, in which the expression of an adipocyte-specific gene was restored in non-adipogenic cells by the elimination of methylated DNA in a regulatory region (4). Because DNA methylation is considered a tight epigenetic change under physiological conditions, it is a suitable mechanism for cells to inhibit the expression of unnecessary genes. It is, however, still to be investigated whether cells in tissues other than cartilage share the same inhibitory mechanism. It is also important to know how the expression of lineage-specific genes is down-regulated in tissue stem cells before differentiation is initiated. Mesenchymal stem cells (MSCs) in bone marrow are tissue stem cells, which can differentiate into multiple mesenchymal cell lineages including chondrogenic cells (5, 6). Because three-dimensional cultures supplemented with growth factors such as TGF-β can induce the chondrogenic differentiation of MSCs (6), there should be a mechanism other than DNA methylation to down-regulate the gene expression of *ChM-I* in undifferentiated MSCs. Modification of the histone tail is another mechanism regulating gene expression. The acetylation of histone H3 and H4 promotes gene expression, whereas deacetylation inhibits the expression (7). The dimethylation of histone H3 at lysine 9 (H3K9) in particular is correlated with DNA methylation and markedly inhibits gene expression (8, 9). These modifications of the histone tail and methylation status determine differentiation (10), and are regulated by several intrinsic histone modifiers including p300 and YY1 (11–13). p300 possesses intrinsic histone acetyltransferase (HAT) activity (11, 12). YY1 is a member of the polycomb group of transcription factors, which establish and maintain transcrip-

* This work was supported by Grants-in-aid for Scientific Research from the Japan Society for the Promotion of Science, from the Ministry of Education, Culture, Sports, Science, and Technology, and from the Ministry of Health, Labor, and Welfare.

[S] The on-line version of this article (available at http://www.jbc.org) contains supplemental Figs. S1 and S2.

[1] To whom correspondence should be addressed: Institute for Frontier Medical Sciences, Kyoto University, 53 Kawahara-cho, Shogoin, Sakyo-ku, Kyoto 606-8507, Japan. Tel.: 81-75-751-4134; Fax: 81-75-751-4646; E-mail: togjun@frontier.kyoto-u.ac.jp.

[2] The abbreviations used are: ChM, chondromodulin; MSC, mesenchymal stem cell; HAT, histone acetyltransferase; HDAC, histone deacetylase; OND, oligonucleotides.

tional silencing by recruiting histone deacetylase (HDAC) (13, 14). These intrinsic factors regulate the epigenetic status and regulate gene expression.

Here we demonstrated that the down-regulation of *ChM-I* expression by DNA methylation is restricted in particular cell types, whereas other cells including MSCs are free from the methylation, and found that expression of the *ChM-I* gene in these cells is reversibly dependent on histone modifications, which are regulated by the net activity of intrinsic histone modifiers, YY1 and p300.

EXPERIMENTAL PROCEDURES

Tissue Specimens and Primary Cultured Cells—Mesenchymal (cartilage, bone, fat, muscle, ligament, and tendon) and non-mesenchymal tissues (nerve, artery, and skin) were obtained from the lower limb of a 56-year-old male who underwent above-knee amputation. The tissues were frozen by dry ice and kept at −80 °C until nucleic acid extraction. Human primary cultured chondrocytes (hPCs) was isolated from same patient and cultured as previously mentioned (15). MSCs were isolated from the iliac bone of healthy donor as described (16). Normal human osteoblasts (NHOSTs) and human primary pre-adipocytes (hPAs) were obtained from TaKaRa (TaKaRa Bio, Shiga, Japan). All the primary cells were maintained in DMEM (Sigma-Aldrich) with 10% fetal bovine serum (Thermo Fisher Scientific Inc., Waltham, MA), 100 units/ml penicillin, and 100 mg/ml streptomycin, in 5% CO_2 at 37 °C. The Ethics Committee of the Faculty of Medicine, Kyoto University, approved the procedure and informed consent was obtained.

Cell Lines and Culture Conditions—The human cell lines, Saos2, were obtained from American Type Culture Collection (ATCC; Manassas, VA). The human osteosarcoma cell lines TAKAO and ANOS were established in our laboratory (2). All the cell lines used in this study were maintained in DMEM (Sigma-Aldrich) with 10% fetal bovine serum (Thermo Fisher Scientific Inc.), 100 units/ml penicillin, and 100 mg/ml streptomycin, in 5% CO_2 at 37 °C.

Antibodies and Expression Vectors—The following antibodies were used; anti-YY1 (sc-7341, Santa Cruz Biotechnology, Santa Cruz, CA), anti-p300 (05–257, Millipore Corp, Billerica, MA), anti-Sp3 (sc-644, Santa Cruz Biotechnology), anti-acetylated H3K9 (06–942, Millipore Corp), anti-dimethylated H3K9 (07–212, Millipore Corp), anti-pan H3 (07–690, Millipore Corp), and anti-HDAC2 (51–5100, Zymed Laboratory Inc., San Francisco, CA). Expression vectors for YY1 (pCEP-YY1) and p300 (pcDNA3-p300) were kindly provided by Drs. E. Seto and K. Miyazono, respectively. The Sp3 expression vector (pCMV-Sp3) was previously described elsewhere (17).

Reverse Transcription (RT)-PCR and Quantitative RT-PCR—RNA was isolated using the Rneasy kit (Qiagen KK, Tokyo, Japan) from frozen tissues and the cultured cell lines. All RT reactions were performed using 1 μg of total RNA with a Super Script First Strand Synthesis System for RT-PCR kit (Invitrogen, Carlsbad, CA). The relative amount of *ChM-I* mRNA was assessed by TaqMan real-time PCR with the ABI PRISM 7700 sequence detection system (Applied Biosystems, Foster City, CA) (2). A75-bp fragment from +411 (exon 4) to +485 (exon 5) of the *ChM-I* cDNA (GenBank™ accession number XM_007132) was amplified using specific primers (sense, 5′-GAAGGCTCGTATTCCTGAGGTG-3′; antisense, 5′-TGGCATGATCTTGCCTTCCAGT-3′) and labeled with a TaqMan probe (5′-FAM-CGTGACCAAACAGAGCATCTC-CTCCA-3′-TAMRA). 18 S rRNA was used as the internal control, and all reactions were run in duplicate. The ratio of *ChM-I*/18 S in each sample was calculated, and the expression level of *ChM-I* genes was demonstrated as a relative value using the *ChM-I*/18 S ratio in human articular cartilage as a standard (1.0) (2).

Drug Treatment—Cells (1×10^5) were seeded on 60-mm dishes in DMEM with 10% FBS. After they had attached to the dish, the cells were treated with either 5-*aza*-2′-deoxycytidine (5-*aza*-dC; Sigma-Aldrich) (1 μM) for 96 h or MS-275 (Nihon Scherring K.K., Chiba, Japan) (1 μM) for 24 h.

Bisulfite Genomic Sequencing—The bisulfite modification of DNA samples was performed using the EpiTect bisulfite kit (Qiagen). DNA (1 μg) was digested by BamHI for 12 h and subjected to sodium bisulfite treatment. Bisulfite-modified DNA-spanning residues −297 to −104 relative to the transcription start point (2) was amplified, cloned into the TA-vector (Invitrogen), and sequenced using an ABI 377 semiautomatic sequencer (Applied Biosystems).

Electrophoresis Mobility Shift Assay (EMSA)—Double-stranded DNA fragments corresponding to the sequence from −357 to −333 and from −86 to −44 were synthesized by annealing two single-stranded oligonucleotides (OND) (5′-CTTCACCTTCCATGAGCCATCTTC-3′ and 5′-GGGGGA-AGATGGCTCATGGAAGGT-3′; 5′-GGGCATCCGGGAG-TGCAGGACGAGCTTCCCGCGGCGGGA-3′; and 5′-TCT-CTCCCGCCGCGGGAAGCTCGTCCTGCACTCCCGGAT-3′, respectively) and filling in by DNA polymerase I (TOYOBO, Osaka, Japan). These fragments were designated GR3 and GR4 (Fig. 2*B*). For the formation of the complex, 5 μg of nuclear extract from cell lysate was incubated with ^{32}P end-labeled ONDs for 20 min at room temperature. The mixtures were electrophoresed in 5% polyacrylamide gel in 0.5× Tris borate EDTA at 45 volts for 3 h, and the gel then was dried and autoradiographed. For the competition assay, the OND-protein complex was produced in the same way in the presence of given amounts of non-labeled OND. In the supershift assay, nuclear extracts were incubated with 1 μg of anti-YY1 and anti-p300 antibody for 1 h on ice before being mixed with labeled DNA.

Luciferase Assay—The 533-bp fragment from −446 to +86 and 383-bp fragment from −296 to +86 relative to the transcription initiation site of the *ChM-I* gene was amplified by PCR, and cloned into a TA-vector using the TOPO cloning kit (Invitrogen). These fragments were subcloned into the luciferase reporter plasmid, PGV-B (Toyo Ink, Tokyo, Japan), yielding PGV-B-f1 and PGV-B-f1-del. Two tandem binding motifs of YY1 (*CC*AT) was mutated to (*TT*AT) by PCR, cloned into PGV-B, and designated PGV-B-f1-mt. One microgram of each reporter plasmid was co-transfected with 1 μg of pCEP-YY1 or pCMV-p300. Transfection efficiency was standardized by the co-transfection of 1 ng of pRL-TK control vector (Toyo Ink). Cells were harvested 24 h after transfection, and luciferase assays were performed with the

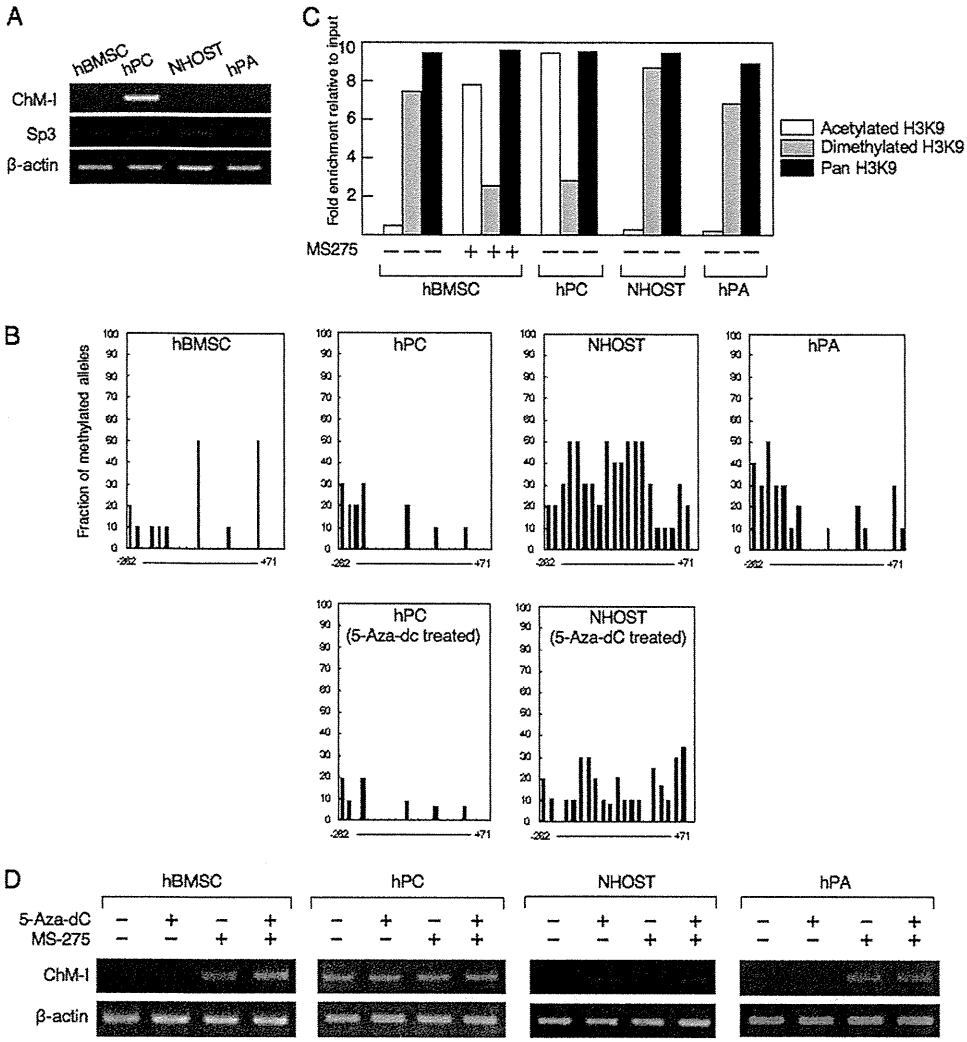

FIGURE 1. **DNA methylation and histone deacetylation down-regulate the expression of *ChM-I* in a cell type-specific manner.** *A*, expression of the *ChM-I* and *Sp3* genes in primary cultured mesenchymal cells. *B*, methylation status of the core-promoter region of *ChM-I*. The methylation of each CpG site was analyzed in 10 alleles by bisulfite genomic sequencing. The *y*-axis indicates the fraction of methylated alleles and the *x*-axis indicates the position of each CpG site relative to the transcription start site. Methylation status in hPC and NHOST treated with a demethylating reagent (5-*aza*-dC, 1 μM for 96 h) were also shown. *C*, ChIP-qPCR assay for the modification of histones in primary cultured mesenchymal cells. *Open box*, acetylated H3K9; *closed box*, dimethylated H3K9; *gray box*, Pan H3. Histone modification in hBMSC treated with an HDAC inhibitor (MS-275, 1 μM for 24 h) were also shown. The *y*-axis represents fold enrichment relative to input. *D*, expression of *ChM-I* after treatment with 5-*aza*-dC and/or MS-275.

PicaGene Dual SeaPansy system (Toyo Ink). Firefly-luciferase activity and SeaPansy-luciferase activity were measured as relative light units with a luminometer (STRATEC Biomedical Systems, Birkenfeld, Deutschland). The fold increase was calculated based on empty vector activity. Each experiment was performed in triplicate.

Chromatin Immunoprecipitation-Quantitative Polymerase Chain Reaction—The suitability of each antibody for the ChIP assay was confirmed by immunoprecipitation-Western blotting (data not shown). Tissue samples were treated using an EpiQuik tissue ChIP kit (Epigentek Group Inc. Brooklyn, NY). Cells were harvested and mixed with formaldehyde at a final concentration of 1.0% for 10 min at 37 °C to cross-link protein to DNA. Cells then were suspended in 0.2 ml of SDS lysis buffer and settled on ice for 10 min. DNA cross-linked with protein was sonicated into fragments of 200–1,000 bp. One-tenth of the sample was set aside as an input control, and the rest was precleared with salmon sperm DNA protein A-Sepharose beads (Millipore Corp) for 30 min with agitation. The soluble chromatin fraction was collected with each antibody at 4 °C overnight with rotation. Immune complexes were collected with salmon sperm DNA protein A-Sepharose beads and washed with the manufacturer's low salt, high salt, and LiCl buffers and then washed twice with TE buffer (10 mM Tris-HCl and 1 mM EDTA). The chromatin-antibody complexes were eluted with elution buffer (1% SDS and 0.1 M $NaHCO_3$). Protein DNA cross-links were reversed with 5 M NaCl at 65 °C for 4 h, proteinase K treatment and phenol-chloroform extraction were carried out, and then the DNA was precipitated in ethanol. The DNA pool from ChIP, input control and negative control was used for quantitative PCR. PCR amplification was performed on an ABI 7700 real-time PCR (Applied Biosystems). PCR amplification was performed using primers specific for the *ChM-I* regulatory region (sense, 5′-GAATGCAGGCCAGTGAGAAGGT-3′;1 antisense, 5′-GCACCCTGGGATCTGTCCCGCT-3′, Fig. 2*B*). The PCR conditions were an initial step of 5 min at 95 °C, followed by 40 cycles of 15 s at 95 °C, 10 s at 64 °C and 60 s at 72 °C. Primers were designed according to the selected genes for evaluating ChIP. To generate a standard curve for each amplicon, threshold cycle (CT) values of serially diluted input DNA, which were extracted in the ChIP experiment, were determined. The status of histone modification and binding of HDAC2, p300, YY1, and Sp3 changes were determined using the 2(-Delta Delta C(T)) method (18). They were demonstrated as a relative value using the enrichment of IP DNA/input DNA. A melting curve analysis was performed for each reaction to ensure a single peak. Each experiment was performed in triplicate, with the values averaged to obtain 1 datum per sample.

siRNAs—Luciferase siRNA duplex (GL2RN1, Dharmacon) was used as a negative control. 40 μM siRNA for YY1 (GeneSolution siRNA; Hs-YY1–5, Qiagen), p300 (p300 Pub. siRNA, Duplex1, Qiagen), and Sp3 (previously described in (2)) were transfected by Lipofection LTX (Invitrogen). RNA was prepared 48 h after transfection and used for the RT-PCR.

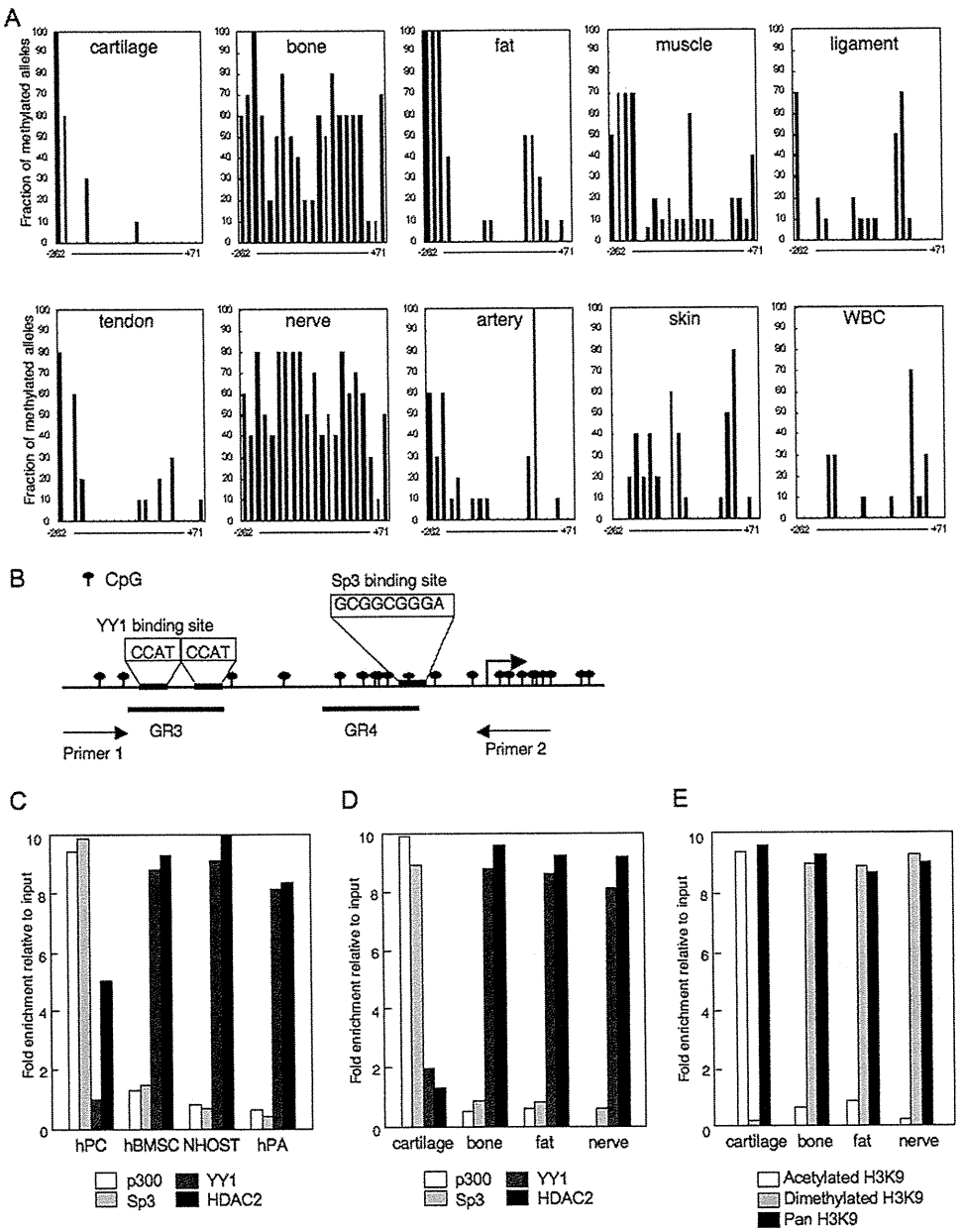

FIGURE 2. **Binding of YY1 and p300 determined the modification of H3K9 and the mRNA expression of *ChM-I* in mesenchymal tissues.** *A*, methylation status of the core-promoter region of the *ChM-I*. DNA extracted from normal tissue was analyzed by bisufite genomic sequencing. *B*, genomic structure of the core-promoter region of *ChM-I*. CpG sites from −262 to +71 were marked as indicated, and the transcription start site is indicated by an *arrow*. Two overlapping YY1-binding motifs (−344 to −347 and −342 to −346), and an Sp3-binding motifs (−56 to −48) are also indicated. A DNA fragment for the ChIP assay was amplified by primer 1 (−446 to −425) and primer 2 (+70 to +91). GR3 (−357 to −337) and GR4 (−86 to −44) were OND probes used in the EMSA for YY1 and p300, respectively. ChIP-qPCR assay for the binding of transcriptional regulators in primary cultured cells (*C*) and cells of normal tissues (*D*). The *y*-axis represents fold enrichment relative to input. *E*, ChIP-qPCR assay for the modification of histones in normal tissues.

RESULTS

DNA Methylation and Histone Deacetylation Down-regulate the Expression of ChM-I in a Cell Type-specific Manner—The expression of *ChM-I* was analyzed by RT-PCR in primary-cultured mesenchymal cells (hMSCs, hPCs, NHOSTs, and hPAs), among which only hPCs expressed the gene (Fig. 1*A*). We have previously shown the expression of *ChM-I* to be induced by the binding of Sp3, which was regulated by the methylation status of the binding motif in the core-promoter region (2). Expression levels of the *Sp3* gene did not differ among the four types of cells (Fig. 1*A*). The core-promoter region of *ChM-I* was hypomethylated in hPCs and hypermethylated in NHOSTs (Fig. 1*B*), which was consistent with the positive and negative expression of *ChM-I* in each cell. The methylation status of the core-promoter region of hMSCs or hPAs, however, was not significantly different from that of hPCs in spite that the expression of *ChM-I* was not detected in these cells (Fig. 1*B*). We have also shown that the acetylation of histone H3 at lysine 9 (H3K9) is necessary to induce the binding of Sp3 to the core-promoter region of *ChM-I*. ChIP analyses showed that H3K9 associated with the core-promoter region was acetylated in hPCs, but dimethylated in hMSCs, NHOSTs, and hPAs (Fig. 1*C*). Treatment with a demethylation reagent (5-*aza*-dC) induced the expression of *ChM-I* in NHOSTs (Fig. 1*D*), which was associated with demethylatiion in the promoter region of the *ChM-I* gene (Fig. 1*B*, *lower panel*). 5-*aza*-dC treatment, however, showed no effects in hMSCs or hPAs (Fig. 1*D*). On the other hand, treatment with a HDAC inhibitor (MS-275) induced the expression of *ChM-I* gene in hMSCs and hPAs, but not in NHOSTs (Fig. 1*D*). The induction of ChM-1 gene expression in hMSC was associated with the acetylation of H3K9 (Fig. 1*C*). These results suggested two mechanisms for the down-regulation of *ChM-I* expression in primary-cultured cells; methylation of the core-promoter region as found in NHOSTs, and histone deacetylation and methylation without DNA methylation as found in hMSCs and hPAs.

The Binding of YY1 and p300 Correlates to the Expression of ChM-I in Normal Mesenchymal Tissues—Among the normal mesenchymal tissues examined, the expression of *ChM-I* was observed only in cartilage (supplemental Fig. S1). The methylation status of the core-promoter region, however, differed significantly among tissues (Fig. 2*A*). DNA extracted from cells in cartilage and fat tissues showed a hypomethylated state in the core-promoter region, which was similar to those found in hPCs and hPAs (Fig. 1*B*). DNA extracted from cells in bone and nerve tissues showed

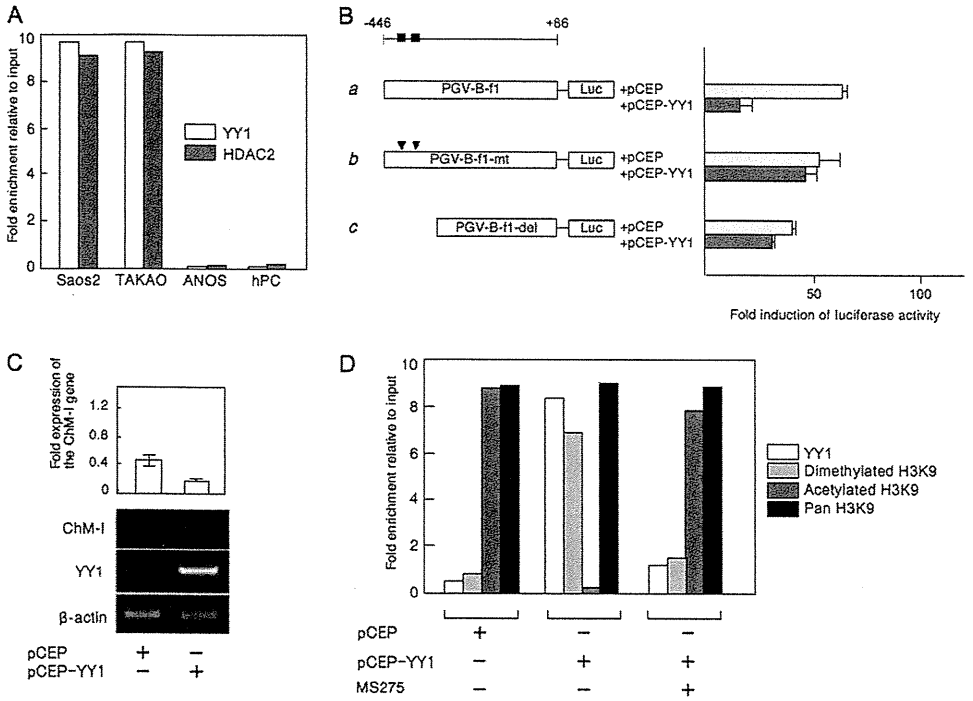

FIGURE 3. **YY1 bound to the regulatory region of *ChM-I* and decreased the promoter activity of *ChM-I*.** *A*, ChIP-qPCR assay for YY1 and HDAC2. *B*, luciferase reporter assay. *a*, DNA fragment encompassing −446 to +86 was cloned into a reporter vector containing the luciferase gene (*PGV-B-f1*). The *black box* indicates the location of the consensus sequence for the YY1-binding motif. *b*, PGV-B-f1-mt contains mutations in the YY1-binding motif (*arrowhead*), and PGV-B-f1-del lacked the YY1-binding motifs (c). Each reporter vector was co-transfected with empty vector (*pCEP*) or the YY1 expression vector (*pCEP-YY1*) into ANOS. The fold-increase was calculated based on empty vector activity. *C*, expression of endogenous *ChM-I* in hPCs transfected with the YY1 expression vector. The expression of *ChM-I* was semi-quantified taking the value for endogenous expression as 1.0 and is demonstrated at the *top*. *D*, ChIP-qPCR assay of hPCs transfected with the YY1 expression vector with or without MS275 treatment (1 μM for 24 h). Forced expression of YY1 in hPCs changed the modification of the H3 tail from acetylation to dimethylation.

that the core-promoter region was hypermethylated, which was similar to those that found in NHOSTs (Fig. 1*B*). In other tissues, the core-promoter region was hypomethylated. These results further suggested a mechanism other than DNA methylation to down-regulate the expression of *ChM-I*.

A search for factors regulating the chromatin structure revealed two tandem repeats (−344 to −347 and −342 to −346) of the binding motif of YY-1, which represses gene expression by recruiting HDAC to target regions (13, 14). As for factors with HAT activity, we focused on p300, which is known to relieve the transcriptional repression by YY1 (19). p300 also plays a role as a transcriptional adaptor recruiting transcription factors such as Sp3 (20). ChIP-qPCR assay showed that YY1 and HDAC2 bound to the core-promoter region in ChM-I-negative hMSCs, NHOSTs, and hPAs, whereas p300 and Sp3 bound in ChM-I-positive hPC (Fig. 2*C*). Consistent with the results obtained with primary-cultured cells, p300 and Sp3 bound to the core-promoter region in cells of cartilage, but not bone, fat or nerve tissue (Fig. 2*D*). On the other hand, the binding of YY1 and HDAC2 was observed in cells of bone, fat, and nerve, but not cartilage (Fig. 2*D*). ChIP-qPCR assay of the histone tail associated with the core-promoter region demonstrated that H3K9 was acetylated in cells of cartilage tissue, and dimethylated in those of bone, fat, and nerve tissues (Fig. 2*E*), which corresponded with the expression of *ChM-I* in each tissue. These results indicated that the expression of *ChM-I* correlated positively with the binding of p300 and negatively with that of YY1.

YY1 Binds to the Core Promoter Region and Inhibits Transcription—To further analyze the involvement of YY1 and p300 in the regulation of *ChM-I*, we used an osteosarcoma cell line, ANOS, as a ChM-I positive cell line, which we have previously investigated. The core-promoter region of the gene was hypomethylated in ANOS cells (2). As ChM-I-negative cell lines, two other osteosarcoma cell lines, Saos2 and TAKAO, were used, in which the core-promoter region was hypermethylated (2).

ChIP-qPCR assays showed that YY1and HDAC2 bound to the regulatory region of Saos2 and TAKAO cells, but not ANOS cells and hPCs (Fig. 3*A*). The binding of YY1 was further confirmed by an EMSA using an oligonucleotide (OND) (GR3) containing putative YY1-binding motifs (−342 to −347) (supplemental Fig. S2*A*). A shifted band was detected in the protein-OND complex from Saos2 cells, which disappeared on competition with unlabeled OND (supplemental Fig. S2*A*, *left panel*). The shifted band was detected also in the protein-OND complex from TAKAO cells, but not in ChM-I-positive cells (ANOS cells and hPCs) (supplemental Fig. S2*A*, *middle panel*). The shifted band was further shifted by the pretreatment with anti-YY1 antibody (supplemental Fig. S2*A*, *right panel*). These results indicated that YY1 bound to the core-promoter region of *ChM-I* in ChM-I-negative cells. To analyze the functional involvement of YY1, a reporter assay using the promoter fragment (−446 to +86) was performed (Fig. 3*B*), which contained the basal transcriptional activity of *ChM-I* (2). When the YY1 expression vector was co-transfected with the reporter plasmid, the promoter activity was significantly inhibited in ANOS cells (Fig. 3*B*, *a*). This inhibitory effect of YY1 was not observed when the reporter vector was replaced with one containing mutations in the YY1 motif (Fig. 3*B*, *b*) or lacking the motif (Fig. 3*B*, *c*). Forced expression of YY1 inhibited the expression of the endogenous *ChM-I* gene in hPCs (Fig. 3*C*), which was associated with the deacetylation and dimethylation of H3 (Fig. 3*D*). Co-treatment with MS275 inhibited the effect of forced expression of YY-1, rescuing the acetylation of H3K9 (Fig. 3*D*). These results suggested that YY1 inhibits the transcriptional activity of *ChM-I* by binding to a putative binding motif in the core-promoter region.

p300 Binds to the Core Promoter Region and Enhances Transcription—ChIP-qPCR assays showed that p300 as well as Sp3 bound to the core-promoter region of *ChM-I* in ANOS cells and hPCs, but not Saos2 and TAKAO cells (Fig. 4*A*). H3K9 associated with this region was acetylated in ANOS cells and

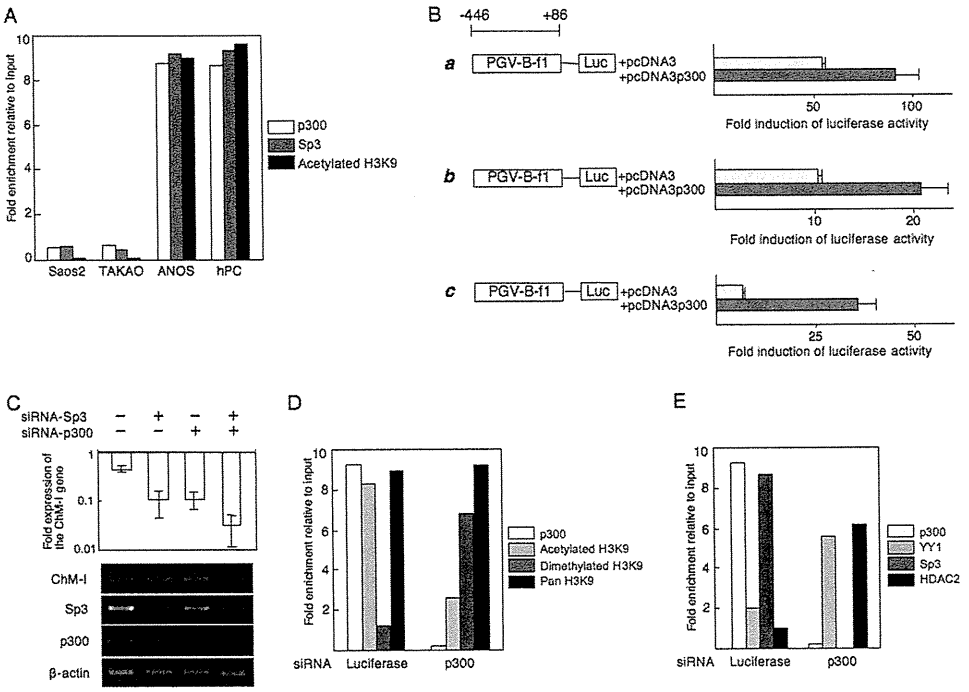

FIGURE 4. **p300 binds to the core promoter region and enhances transcription.** *A*, ChIP-qPCR assay of p300, Sp3 and acetylated H3. *B*, luciferase reporter assay. The reporter construct was described in the legend for Fig. 3*B*, and co-transfected with empty vector (pcDNA3) or the p300 expression vector (pcDNA3-p300) into ANOS (*a*), Saos2 (*b*), or TAKAO (*c*). The fold-increase was calculated based on empty vector activity. *C*, down-regulation of ChM-I gene expression by siRNA for Sp3 and/or p300. siRNAs for Sp3 and/or p300 were transfected into ANOS, and the expression of ChM-I, Sp3, and p300 was analyzed by RT-PCR. The expression of *ChM-I* was semi-quantified taking the value for endogenous expression as 1.0 and is demonstrated at the *top*. *D*, ChIP-qPCR assay for the modification of H3K9 (*D*) and for the binding of transcription regulators (*E*): cross-linked DNA-protein complexes were prepared from ANOS treated with or without siRNA for p300 and used for ChIP-qPCR assay.

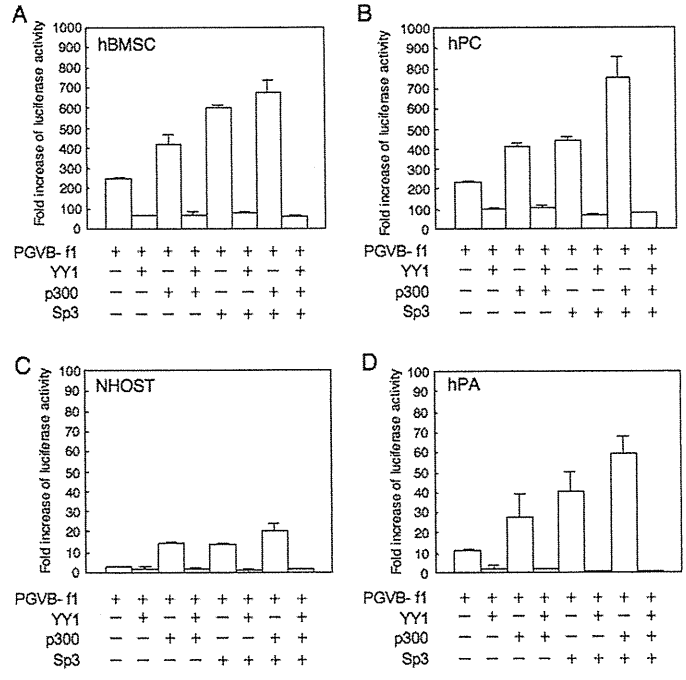

FIGURE 5. **Promoter activity of *ChM-I* was promoted by Sp3 and p300, but completely inhibited by YY1 in primary cultured cells.** The luciferase reporter vector containing the core-promoter fragment of the *ChM-I* gene (*PGV-B-f1*) was co-transfected with YY1, p300 and/or Sp3 expression vectors into hMSCs (*A*), hPCs (*B*), NHOSTs (*C*), and hPAs (*D*). The fold-increase was calculated based on empty vector activity.

hPCs, but not Saos2 or TAKAO cells (Fig. 4*A*). The binding of p300 was further confirmed by an EMSA using an OND (GR4)-containing putative p300 and Sp3-binding motifs (−56 to −48) (supplemental Fig. S2*B*). A shifted band was observed in extracts from ANOS cells, but not Saos2 or TAKAO cells (supplemental Fig. S2*B*, *middle panel*). The specificity of the band was confirmed by addition of a cold OND (supplemental Fig. S2*B*, *left panel*). The shifted band was supershifted when cell extracts were pretreated with anti-Sp3 antibody, and the same band disappeared when cell extracts were pretreated with anti-p300 antibody (supplemental Fig. S2*B*, *right panel*), suggesting that the protein-OND complex contained both Sp3 and p300. The functional involvement of p300 was analyzed with a promoter assay. Promoter activity was increased by co-transfection of the p300 expression vector in both ChM-I-positive (ANOS, Fig. 4*B*, *a*) and negative (Saos2, Fig. 4*B*, *b*; TAKAO, Fig. 4*B*, *c*) cells. Inhibition of p300 or Sp3 expression by the siRNA for each gene (siRNA-p300 and siRNA-Sp3) reduced the expression of *ChM-I* in hPCs, while the two siRNAs combined had an additive effect (Fig. 4*C*). ChIP-qPCR assays showed that the siRNA for p300 changed H3K9 from an acetylated to dimethylated form (Fig. 4*D*). These results suggest that p300 positively regulates the transcriptional activity of *ChM-I* by inducing the acetylation of H3K9 associated with this region.

Involvement of YY1 and p300 in Primary Mesenchymal Cells—The effect of YY1 and p300 on promoter activity was further analyzed in primary-cultured mesenchymal cells (Fig. 5). Surprisingly, the transcriptional activity of the basal promoter fragment in hMSCs (Fig. 5*B*) was as strong as those in hPCs (Fig. 5*A*), although the expression of endogenous *ChM-I* was weak in hMSCs. In contrast, the basal activity level was low in NHOSTs and hPAs (Fig. 5, *C* and *D*). When the YY1 expression vector was co-transfected with the reporter vector, promoter activity was significantly inhibited in all strains (Fig. 5, *A–D*). Co-transfection with the p300 or Sp3 expression vector enhanced the activity, and simultaneous transfection of the two vectors increased it in an additive manner (Fig. 5, *A–D*). The enhancement of *ChM-I* expression by the p300 and/or Sp3 expression vectors was completely inhibited by the co-transfection of YY1 in all strains (Fig. 5, *A–D*). These results confirmed that YY1 and p300 are involved in the regulation of *ChM-I* transcription in mesenchymal cells, and that because this luciferase reporter system has no relationship with histone modifications, YY1

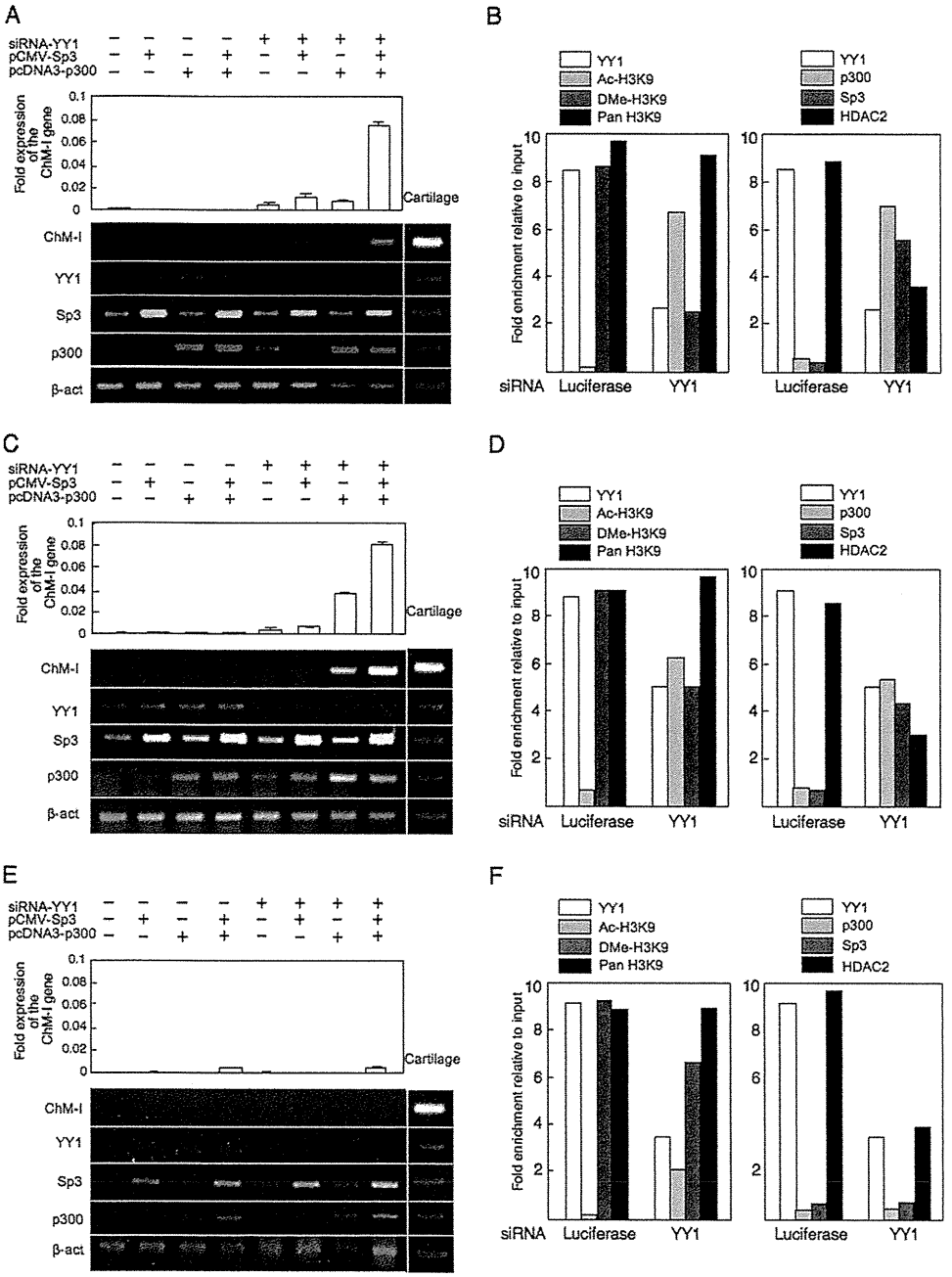

FIGURE 6. **Induction of *ChM-I* expression in ChM-I-negative primary cultured cells by modification of regulators.** *A–C*, primary-cultured cells were transfected with a combination of the siRNA for YY1, p300 expression vector, and Sp3 expression vector, and mRNA level of *ChM-1*, *YY1*, *p300*, and *Sp3* gene were analyzed by semi-quantitative RT-PCR (*lower panel*). The expression of the *ChM-I* was further analyzed by quantitative RT-PCR and digitalized (*upper panel*). *A*, hMSCs; *C*, hPAs; *E*, NHOSTs. ChIP-qPCR assay: *B*, hMSCs; *D*, hPAs; *F*, NHOSTs. Cross-linked DNA-protein complexes were prepared from primary cultured cells treated with or without siRNA for YY1 and used for ChIP-qPCR assay for the modificationf H3K9 (*left panels*) and for the binding of transcription regulators (*right panels*).

may directly inhibit the function of p300 or p300/Sp3 complex in addition to the modification of chromatin structure.

Cell-specific Effects of YY1 Inhibition on the Expression of ChM-I—Finally, the effect of YY1 expression on endogenous ChM-I expression was evaluated using siRNA for the gene (siRNA-YY1). In hMSCs (Fig. 6*A*), the inhibition of YY1 expression slightly induced the expression of *ChM-I* gene. The introduction of the p300 and/or Sp3 expression vectors had little effect on the expression of *ChM-I*, but significantly up-regulated it when combined with siRNA-YY1. Similar results were obtained in hPAs (Fig. 6*C*). In both cell types, siRNA-YY1 treatment induced the acetylation of H3K9 along with reductions in the dimetylation of H3K9 (Fig. 6, *B* and *D*, *left panels*). At the same time, siRNA-YY1 treatment dissociated HDAC2 and recruited p300 and Sp3 in the core-promoter region of *ChM-I* (Fig. 6, *B* and *D*, *right panels*). In NHOSTs (Fig. 6*E*), however, the combination the inhibition of YY1 and over-expression of p300 and Sp3 showed little effect for the induction of *ChM-I* expression. siRNA-YY1 treatment failed to induce the acetylation of H3K9 (Fig. 6*F*, *left panel*). Interestingly, although p300 was successfully recruited to the promoter region, no binding of Sp3 was observed in NHOSTs (Fig. 6*F*, *right panel*). These results suggested that Sp3 and p300 independently bind to the promoter region, and the binding of Sp3 was inhibited by the methylation of target DNA, but that of p300 was not. Therefore, the expression of a cartilage-specific gene, *ChM-I*, can be induced in some types of mesenchymal cells including MSCs by the modification of repressors (YY1) and activators (p300), but not in other cells, in which the expression is irreversibly inhibited by DNA methylation.

DISCUSSION

Numerous studies support the importance of epigenetic status for the regulation of differentiation, based on experiments involving chemical modifications of genome and the winding protein histone (21, 22). DNA methylation at CpG dinucleotides is a major epigenetic modification of the genome and associated with gene silencing (23). Because no intrinsic DNA-demethylating enzyme has been found, the inhibition by DNA methylation is tight under physiological conditions. Genomic DNA of embryonic stem (ES) cells is hypomethylated, and the total amount of methylated DNA increases with development (22, 24). Thus DNA methylation is a key mechanism to regulate and maintain the expression of cell type-specific genes. Unexpectedly, however, the methylation in the core-promoter region played a role in inhibiting the expression of *ChM-I* only

in particular types of mesenchymal cells; cells in bone (mainly osteocytes and osteoblasts) and peripheral nerve (mainly Schwann cells and perineural cells) (Fig. 2*A*). The hypomethylated status in hMSCs is reasonable considering the potential of these cells to differentiate. However, the core-promoter in terminally differentiated cells of a remote cell-lineage such as white blood cells was free from methylation and thus in a reversible state for gene expression (Fig. 2*A*). At present, we have no data to explain why some types of cells use DNA methylation to inhibit the expression of *ChM-I* and others do not. Cells of chondrogenic and osteogenic lineages are closely related, and may share a considerable proportion of transcriptional machinery. Therefore DNA methylation might be required to inhibit the expression of genes specific to chondro- or osteogenic lineages. The reporter assay gave almost identical results in hMSCs as in hPCs (Fig. 5, *A* and *B*), indicating that transcriptional machinery n hMSC to be ready to induce the expression of *ChM-I*, although there is no endogenous expression of the gene. This result strongly suggested that epigenetic machinery regulated the lineage-specific gene expression in stem cells.

The epigenetic status of each cell had been considered static, but recent a study demonstrated a dynamic nature to these modifications (25). We and others gave examples in which modification of the histone code induced a change of DNA methylation (3, 26). Notably, the modification of H3K9 strongly correlated with DNA methylation; dimethylated H3K9 correlated with hypomethylation and deacetylated H3K9 correlated with hypermethylation (9, 27). The recent discovery that the forced expression of transcription factors can reverse the epigenetic status of differentiated to that of ES cells is an extreme example of the dynamic nature of epigenetic status (28, 29). We showed that the expression of *ChM-I* was down-regulated by histone modifications in stem cells and some types of differentiated cells. The epigenetic status is induced and maintained by a number of intrinsic histone modifiers (30). In this study, we found that YY1 and p300 are main modifiers of histone associated with the core-promoter region of the ChM-I gene. YY1 is a DNA-binding zinc finger transcription factor, which has dual functions as an activator and a repressor (14). YY1 inhibits the transcription of target genes by competing for DNA-binding sites with activators, binding directly to activators, or recruiting co-repressors (14). One of these co-repressors is HDAC2, which was first identified as a binding partner of YY1 (13, 14). Previously, we demonstrated that HDAC2 bound to a histone tail associated with the core-promoter region of *ChM-I* in ChM-I-negative cells (3). In the present study, we showed that forced expression of YY1 deacetylated H3 associated with the core-promoter region in *ChM-I* (Fig. 3*E*), whereas HDAC2 was dissociated by the inhibition of YY1, causing acetylation of H3 (Fig. 6, *B*, *D*, and *F*). These results indicated that YY1 repressed the expression of *ChM-I* by recruiting HDAC2 to induce deacetylation of H3. Another repressive mechanism is the direct binding of p300, a binding partner of YY1 (14). p300 acts as an activator for target gene expression through intrinsic HAT activity (11, 12). Inhibition of p300 by siRNA resulted in the deacetylation of H3 and the repression of *ChM-I* expression (Fig. 5*C*), indicating the role of p300 as HAT for *ChM-I* expression. p300 also acts as a transcriptional co-activator for Sp3, not Sp1 (19), which is the main transcription factor of *ChM-I* (2). The exogenous expression of p300 enhanced the promoter activity in the reporter assay, suggesting the role of p300 as a co-activator. Inhibition of the promoter activity by the YY1 expression vector in the reporter assay indicated that YY1 acted as a direct repressor for p300 in addition to acting as a recruiter of HDAC (Fig. 6, *A*, *C*, and *E*). These results suggested that YY1 and p300 are involved in the regulation of *ChM-I* expression through the modification of histones and also the regulation of each others function.

It remains unclear how the repression of YY1 is relieved in chondrogenic cells. One possible mechanism is a post-translational modification of the YY1 protein. YY1 is glycosylated by *O*-linked *N*-acetylglucosaminylation, and glycosylated YY1 fails to bind to DNA (31). *O*-linked glucosamine is expressed in cartilage tissue (32). Such tissue-specific modifications may determine the expression of tissue-specific genes. It is also likely that tissue-specific chromatin-remodeling factors other than YY1 and p300 are involved in the regulation. Analyzing these issues may help to elucidate how the direction of differentiation is determined in stem cells.

Acknowledgments—We thank Dr. M. Nakanishi for providing MS-275 and helpful suggestions, Dr. K. Miyazono for the p300 expression vector, and Dr. E. Seto for the YY1 expression vector.

REFERENCES

1. Hiraki, Y., Tanaka, H., Inoue, H., Kondo, J., Kamizono, A., and Suzuki, F. (1991) *Biochem. Biophys. Res. Commun.* **175,** 971–977
2. Aoyama, T., Okamoto, T., Nagayama, S., Nishijo, K., Ishibe, T., Yasura, K., Nakayama, T., Nakamura, T., and Toguchida, J. (2004) *J. Biol. Chem.* **279,** 28789–28797
3. Aoyama, T., Okamoto, T., Kohno, Y., Fukiage, K., Otsuka, S., Furu, M., Ito, K., Jin, Y., Nagayama, S., Nakayama, T., Nakamura, T., and Toguchida, J. (2008) *Biochem. Biophys. Res. Commun.* **365,** 124–130
4. Noer, A., Sorensen, A. L., Boquest, A. C., and Collas, P. (2006) *Mol. Biol. Cell.* **17,** 3543–3556
5. Caplan, A. I. (1991) *J. Orthop. Res.* **9,** 641–650
6. Pittenger, M. F., Mackay, A. M., Beck, S. C., Jaiswal, R. K., Douglas, R., Mosca, J. D., Moorman, M. A., Simonetti, D. W., Craig, S., and Marshak, D. R. (1999) *Science* **284,** 143–147
7. Grunstein, M. (1997) *Nature* **389,** 349–352
8. Zhao, W., Soejima, H., Higashimoto, K., Nakagawachi, T., Urano, T., Kudo, S., Matsukura, S., Matsuo, S., Joh, K., and Mukai, T. (2005) *J. Biochem.* **137,** 431–440
9. Kondo, Y., Shen, L., and Issa, J. P. (2003) *Mol. Cell. Biol.* **23,** 206–215
10. Gan, Q., Yoshida, T., McDonald, O. G., and Owens, G. K. (2007) *Stem Cells* **25,** 2–9
11. Ogryzko, V. V., Schiltz, R. L., Russanova, V., Howard, B. H., and Nakatani, Y. (1996) *Cell* **87,** 953–959
12. Bannister, A. J., and Kouzarides, T. (1996) *Nature* **384,** 641–643
13. Yang, W. M., Yao, Y. L., Sun, J. M., Davie, J. R., and Seto, E. (1997) *J. Biol. Chem.* **272,** 28001–28007
14. Gordon, S., Akopyan, G., Garban, H., and Bonavida, B. (2006) *Oncogene* **25,** 1125–1142
15. Aoyama, T., Liang, B., Okamoto, T., Matsusaki, T., Nishijo, K., Ishibe, T., Yasura, K., Nagayama, S., Nakayama, T., Nakamura, T., and Toguchida, J. (2005) *J. Bone. Miner. Res.* **20,** 377–389
16. Shibata, K. R., Aoyama, T., Shima, Y., Fukiage, K., Otsuka, S., Furu, M., Kohno, Y., Ito, K., Fujibayashi, S., Neo, M., Nakayama, T., Nakamura, T., and Toguchida, J. (2007) *Stem Cells.* **25,** 2371–2382

17. Suske, G. (1999) *Gene* **238,** 291–300
18. Livak, K. J., and Schmittgen, T. D. (2001) *Methods* **25,** 402–408
19. Lee, J. S., Galvin, K. M., See, R. H., Eckner, R., Livingston, D., Moran, E., and Shi, Y. (1995) *Genes Dev.* **9,** 1188–1198
20. Kishikawa, S., Murata, T., Kimura, H., Shiota, K., and Yokoyama, K. K. (2002) *Eur. J. Biochem.* **269,** 2961–2970
21. Spivakov, M., and Fisher, A. G. (2007) *Nat. Rev. Genet.* **8,** 263–271
22. Bernstein, B. E., Meissner, A., and Lander, E. S. (2007) *Cell* **128,** 669–681
23. Esteller, M. (2007) *Nat. Rev. Genet.* **8,** 286–298
24. Reik, W., Dean, W., and Walter, J. (2001) *Science* **293,** 1089–1093
25. Klose, R. J., and Zhang, Y. (2007) *Nat. Rev. Mol. Cell Biol.* **8,** 307–318
26. Nakao, M. (2001) *Gene* **278,** 25–31
27. Rougeulle, C., Chaumeil, J., Sarma, K., Allis, C. D., Reinberg, D., Avner, P., and Heard, E. (2004) *Mol. Cell. Biol.* **24,** 5475–5484
28. Takahashi, K., Tanabe, K., Ohnuki, M., Narita, M., Ichisaka, T., Tomoda, K., and Yamanaka, S. (2007) *Cell* **131,** 861–872
29. Okita, K., Ichisaka, T., and Yamanaka, S. (2007) *Nature* **448,** 313–317
30. Pasini, D., Bracken, A. P., Agger, K., Christensen, J., Hansen, K., Cloos, P. A., and Helin, K. (2008) *Cold Spring Harb. Symp. Quant. Biol.***73,** 253–263
31. Hiromura, M., Choi, C. H., Sabourin, N. A., Jones, H., Bachvarov, D., and Usheva, A. (2003) *J. Biol. Chem.* **278,** 14046–14052
32. Thonar, E. J., Lohmander, L. S., Kimura, J. H., Fellini, S. A., Yanagishita, M., and Hascall, V. C. (1983) *J. Biol. Chem.* **258,** 11564–11570

Cancer Science
The official journal of the Japanese Cancer Association JCA

A Quantitative trait locus responsible for inducing B-cell lymphoblastic lymphoma is a hotspot for microsatellite instability

Richard H. Kaszynski,[1] Shinya Akatsuka,[2] Takuya Hiratsuka,[3] Guang Jin,[4] Munetaka Ozeki,[1] Tomoko Okuno,[1] Takuro Nakamura,[4] Toshiaki Manabe,[5] Tetsuya Takakuwa,[6] Hiroshi Hiai,[7] Shinya Toyokuni,[2] Keiji Tamaki[1] and Tatsuaki Tsuruyama[1,8]

[1]Department of Forensic Medicine and Molecular Pathology, Graduate School of Medicine, Kyoto University, Kyoto; [2]Department of Pathology and Biological Responses, Graduate School of Medicine, Nagoya University, Nagoya; [3]Department of Pathology, Saisei-kai Noe Hospital, Osaka; [4]Laboratory of Carcinogenesis, Cancer Institute, Tokyo; [5]Department of Diagnostic Pathology, Graduate School of Medicine, Kyoto University, Kyoto; [6]Department of Human Health Science, Graduate School of Medicine, Kyoto University, Kyoto; [7]Shiga Medical Center Research Institute, Shiga, Japan

(Received September 24, 2009/Revised November 2, 2009/Accepted November 4, 2009)

While the molecular mechanisms underlying microsatellite instability (MSI) have been exhaustively investigated, identifying the patterns of MSI distribution within diverse cancer genomes has remained an elusive issue. In the present study, we conducted genome-wide MSI screening in B-cell lymphoblastic lymphomas (B-LBL) which spontaneously develop in the SL/Kh strain of mice. Tumor samples harvested from 16 mice were investigated using a framework map consisting of 150 microsatellite markers spaced at increments of roughly 0.5–3.0 centimorgans, spanning the entirety of mouse chromosomes (mus musculus chromosomes [MMU]) 3–6. MMU3 contains a quantitative trait locus (QTL), *Bomb1* (bone marrow pre-B1), known to induce an aberrant expansion of pre-B cells in bone marrow prior to the onset of B-LBL in SL/Kh mice. The remaining chromosomes were selected on the basis of those most closely resembling MMU3 in terms of total estimated length (maximum variance 10 Mb). MSI was confirmed at 2≤ markers in DNA derived from tumor tissues in 15 SL/Kh mice (93.7%), while healthy splenic DNA samples screened in parallel were consistently negative for MSI. The overall MSI incidence was significantly higher on MMU3 compared with MMU4–6 ($P = 0.031$). Additionally, by applying spatial point pattern analysis combined with a 1-D version of Ripley's *K*-function, we successfully demonstrated the predilection of MSI-susceptible loci to structure a massive cluster within the *Bomb1* locus. Our study is the first to suggest that a QTL concomitantly serves as a hotspot for MSI-susceptible loci and sheds new light on somatic cancer genetics. (*Cancer Sci* 2010; 101: 800–805)

B-cell lymphoblastic lymphomas (B-LBL) are a prototypic high-grade neoplasm composed of immature lymphocytes that demonstrate lymphoblastic morphology and express pan-early B-cell markers.[1–4] As with humans, B-LBL are a relatively rare hematopoietic malignancy in mice.[5]

In our previous studies, we reported on the SL/Kh strain, which is a highly unique cancer model that spontaneously develops lymphomas recapitulating the human entity B-LBL at a high incidence (>90%) and relatively short latency (≤6 months of age).[6–8] An exclusive phenotype associated with the SL/Kh strain is the transient polyclonal expansion of BP-1$^+$B220$^+$ pre B cells in prelymphoma-stage bone marrow (BM), which heralds the development of overt B-LBL.[9,10] A highly significant quantitative trait locus (QTL) responsible for this aberrant expansion of pre-B cells in SL/Kh BM was mapped down to the distal segment of mus musculus chromosome (MMU)3, between 55 centimorgans (cM) (D3Mit300) and 78.5 cM (D3Mit45), and was subsequently termed *Bomb1* (BM pre-B1). In our most recent study, we confirmed that *Bomb1* is in fact responsible for this precursor lesion to B-LBL by constructing a speed congenic strain NFS.SL/Kh–*Bomb1*, in which the *Bomb1* segment of the SL/Kh mouse is introgressed into the genomic canvas of NFS/N mice.[11]

In the course of genotyping this QTL, we encountered a genetic lesion referred to as microsatellite instability (MSI) at high frequencies within the *Bomb1* locus of the SL/Kh lymphoma genome. MSI specificity in tumor cells was first reported in sporadic colorectal tumors,[12,13] and is now widely recognized as a hallmark of defective post-replicative DNA mismatch repair (MMR).[14–16] Since its initial discovery, the presence and frequency of MSI has been exhaustively investigated in a wide spectrum of cancers;[17–25] however, identifying the patterns of MSI distribution within these genomes has never been the object of a thorough examination. Therefore, based on our preliminary findings, we asked ourselves whether the QTL concomitantly serves as a hotspot for MSI-susceptible loci.

To answer this question, we applied a framework map consisting of 150 strategically positioned microsatellites markers at increments of 0.5 to 3 cM to analyze the spatial distribution patterns of MSI within the SL/Kh B-LBL genome. The expected microsatellite mutation rate per locus was a factor considered in erecting the framework map. Hanford *et al.* show that microsatellite mutations accumulate at defined rates per locus per generation in both MMR-proficient (HT-1080, fibrosarcoma) and -deficient (H6, colorectal carcinoma; LoVo, metastatic adenocarcinoma) cancer cell lines.[26] Based on these findings, we reasoned that the overall MSI ratio on chromosomes of equivalent size should be roughly comparable, and selected MMU4, MMU5, and MMU6 as references for our genome-wide assessment after confirming that they display the closest resemblance to MMU3 in terms of total estimated length (maximum variance 10 Mb), as determined via data retrieved from the Mouse Genome Database (MGD).[27] In the present study, we show that the *Bomb1* locus demonstrates markedly increased susceptibility towards MSI accumulation compared with other randomly distributed loci in the SL/Kh lymphoma genome.

Materials and Methods

Animal experiments. Animal experiments were performed with expressed written consent from the Ethics Committee for Animal Experiments, Graduate School of Medicine, Kyoto University (Kyoto, Japan). The origin and genetic properties of SL/Kh and congenic NFS.SL/Kh–*Bomb1* mice have been described

[8]To whom correspondence should be addressed.
E-mail: tsuruyam@kuhp.kyoto-u.ac.jp

doi: 10.1111/j.1349-7006.2009.01437.x

elsewhere.[7,8,11] NFS/N mice have been maintained by sister–brother mating for over 100 generations at the Institute of Laboratory Animals, Kyoto University; SL/Kh mice have been deposited into the National Bio-Resource Project (http://www.anim. med.kyoto-u.ac.jp/nbr/home.htm) at RIKEN (Tsukuba, Japan).

Marker selection. A framework map consisting of 150 polymorphic, microsatellite DNA markers was constructed. Markers were selected to assess the distribution patterns of loci with observed MSI (MSI-susceptible loci) in the SL/Kh genome using MMU3–6 as representative chromosomes. Markers and sequence information for primer pairs were retrieved from the MGD.[27] An intermarker genomic proportion criterion was established to space individual markers at increments of roughly 0.5–3 cM. On sporadic occasions, markers were unavailable to fit within the defined criterion (maximum variance 6.5 cM; MMU6). The markers adopted in this study, along with their chromosomal positions, are provided in the supporting Data S1.

Sample selection. Screening for MSI was performed on B-LBL tissues harvested from 16 SL/Kh mice. Used as the control, DNA isolated from the spleen of SL/Kh mice, the BM of NFS/N, and the congenic strain NFS.SL/Kh–*Bomb1*, were screened in parallel for this study. NFS/N mice are a well-established inbred strain and were selected on the basis of lacking the genetic information of an endogenous ecotropic murine leukemia virus[28] and for having a reportedly low spontaneous incidence of lymphomas and other neoplastic growths.[29] Splenic tissue was selected for the SL/Kh strain on the basis of being a highly vascular lymphoid organ responsible for producing lymphocytes and for having an inherent sensitivity to hematopoietic disorders, such as leukemia and lymphoma. In contrast, BM was selected for the congenic strain, given that the introgressed SL/Kh *Bomb1* segment gives rise to an expansion of pre-B cells in BM resembling the precursor lesion to overt lymphoma development in SL/Kh mice.[11] Additionally, the NFS/N strain serves as the foundation in which the congenic mouse was developed upon, and therefore, BM was similarly adopted as a control for the NFS/N strain.

DNA extraction and isolation. Genomic DNA was extracted from the spleen, lymphoma, and BM using a QIAamp minikit (Qiagen, Valencia, CA, USA) according to the manufacturer's recommended protocol. Following extraction and isolation, DNA obtained from these methods were subjected to polymerase chain reaction (PCR), according to previously described methods.[9,11]

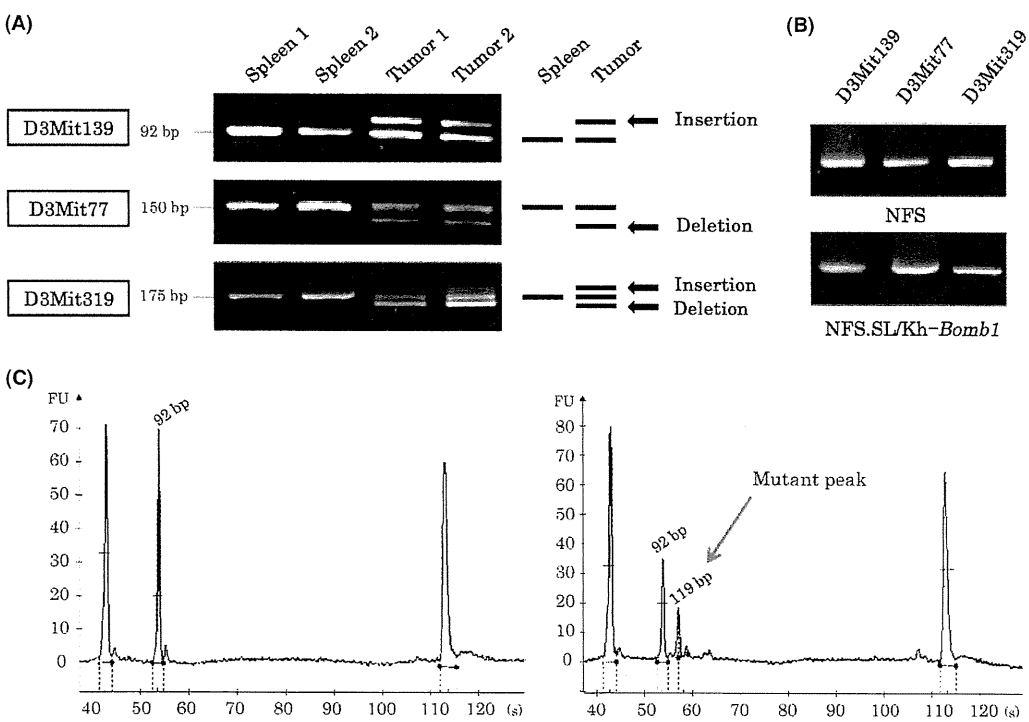

Fig. 1. Microsatellite instability (MSI) screening in SL/Kh B-cell lymphoblastic lymphomas. (A) MSI screening via 3% agarose gel electrophoresis. Agarose gel results obtained at three microsatellite markers showing three variant representations of MSI: insertion mutations resulting from the gain of simple repetitive sequences obtained at marker D3Mit139 (top), deletion mutations (the loss of simple repetitive sequences) observed at marker D3Mit77 (middle), and insertion/deletion mutations (the simultaneous presentation of both insertion and deletion mutations) observed at marker D3Mit319 (bottom). Lanes 1 and 2, SL/Kh spleen-derived polymerase chain reaction (PCR) amplicons from two separate mice (mouse no. 202 and 211).Approximate band sizes are given for healthy control amplicons. Lanes 3 and 4, SL/Kh tumor-derived PCR amplicons demonstrating partial band shifting (mouse no. 202 and 211). (B) Examples of microsatellite stability represented by the external control strains: NFS/N (top) and NFS.SL/Kh-Bomb1 (bottom). Both strains failed to exhibit MSI at any of the examined loci, despite the fact that the introgressed SL/Kh *Bomb1* segment in the NFS.SL/Kh–*Bomb1* strain results in an aberrant polyclonal pro-B cell expansion in bone marrow, mirroring the precursor lesion to lymphomagenesis in SL/Kh mice. Results are shown for markers D3Mit139, D3Mit77, and D3Mit319. (C) Representative allelic profile of SL/Kh spleen and tumor specimens at marker D3Mit139, as analyzed via capillary electrophoresis. Vertical and horizontal scales represent peak fluorescence intensity in relative fluorescence units (FU) and an estimate of PCR product size in base pairs (bp), respectively. The two flanking peaks in each electropherogram are size markers placed at 15 and 1500 bp. Amplicons obtained using normal (splenic) SL/Kh DNA as the template (left). PCR product obtained from tumor DNA showing mutant peak (right; arrow). In normal DNA, a single, dual-intensity homozygous peak is observed, while in tumor amplicons, partial peak shifting is observed and FU is reduced to approximately half the intensity seen in normal tissue.

MSI screening and confirmation. PCR amplicons were subjected to two modes of confirmation for MSI: standard electrophoresis using 3% agarose gel and PCR capillary electrophoresis (Agilent 2100 Bioanalyzer, Palo Alto, CA, USA). The MSI status was established by the presence or absence of aberrant products manifesting in the form of extra bands or peaks, and individually confirmed by two examiners. PCR products with established MSI statuses were further examined under bidirectional sequencing using an ABI3100 automated sequencer and BigDye v3.1 terminators (Applied Biosystems, Foster City, CA, USA) (data not shown).

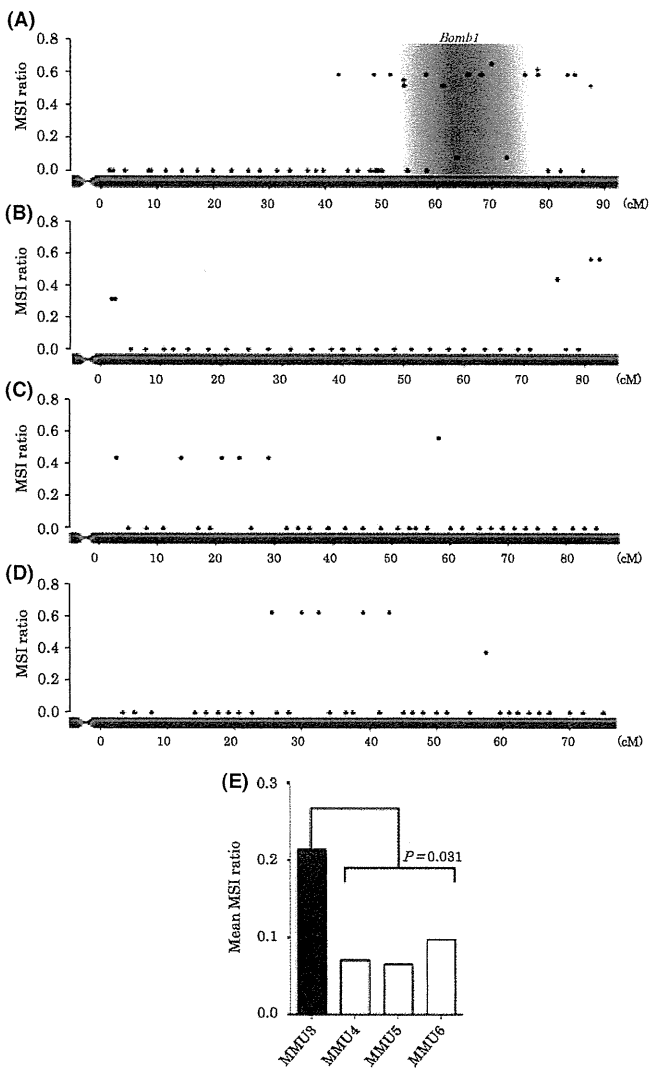

Fig. 2. Transchromosomal comparison of microsatellite instability (MSI) incidence. MSI incidence for each microsatellite marker examined is obtained by dividing the number of MSI-positive samples by the total number of typed lymphoma samples (n = 16). Plots are designed to reflect approximate chromosomal position of each individual microsatellite marker investigated in this study. MSI distribution is shown for the four mouse chromosomes investigated: (A) mus musculus chromosome (MMU)3, (B) MMU4, (C) MMU5, (D) MMU6. *Bomb1* is shaded in gray. Data plots for markers D3Mit300 (55 cM) and D3Mit45 (78.5 cM) representing the boundaries for the *Bomb1* locus are identified on MMU3 with symbols + and *, respectively. Overall MSI incidence was determined for each chromosome by calculating the combined average incidence of MSI per marker on each chromosome (E). cM, centimorgans.

Statistical analysis. To investigate the associations between MSI clustering and the QTL, we applied standard descriptive statistics to characterize data sets. For the comparison of sample groups, a two-tailed Mann–Whitney U-test was used to evaluate statistical significance. A P-value <0.05 was considered to be statistically significant.

***K*-function analysis.** To analyze the distribution patterns of MSI-susceptible loci, we applied a 1-D version of Ripley's K-function.[30] The K-function describes the extent to which there is spatial dependence in the arrangement of events.[31] It is highly useful in identifying the scales at which the spatial point pattern is regarded as significantly underdispersed (clustered) or overdispersed (regular). A certain measure of incidence of MSI at a marker corresponds to an 'event' or point in our study. The K-function analysis is based on distances between all pairs of events, and the function for a point process is defined by:

$$K(t) = \lambda^{-1} E[\text{number of further events within distance } t \text{ of an arbitrary event}] \quad (1)$$

where λ is the intensity, or mean number of events per unit area, and $E[x]$ denotes the expectation of a random variable, x.

Accordingly, the test statistic of $K(t)$ for our analysis was calculated as follows:

$$K(t) = \lambda^{-1} n^{-1} \sum_{i=1}^{n} \sum_{\substack{j=1 \\ (j \neq i)}}^{n} It(u_{ij}) = ln^{-2} \sum_{i=1}^{n} \sum_{\substack{j=1 \\ (j \neq i)}}^{n} It(u_{ij}) \quad (2)$$

where n is the total number of markers susceptible to MSI, l is the combined length (cM) of the four examined chromosomes, u_{ij} is the distance (cM) between points i and j, and $I_t(u)$ and the counter function equals 1 if $u \leq t$ and equals 0 if $u > t$, respectively. For this calculation, we considered the markers of which the rate of MSI incidence was >0.3 as genomic points susceptible to MSI. Since chromosomes are spatially separated, the value of u_{ij} was set to infinite where points i and j represent markers on different chromosomes.

The null hypothesis for our analysis is that every microsatellite locus has an equal probability of showing MSI. Monte Carlo simulation was used to evaluate the significance of deviation from the null hypothesis. The null hypothetical point pattern was realized by randomly choosing n markers among the 150 microsatellite markers that we actually examined.[32] Subsequently, the $K(t)$ for the null hypothetical point pattern was calculated. This was done 1000 times to generate the null distribution. The 95% simulation envelope are the 2.5 and 97.5 percentiles in the null distribution of $K(t)$ for each distance, t.

The values of $K(t)$ can be standardized with the simulated null-distribution as follows:

$$K_{st}(t) = \{K(t) - K_m(t)\}/\sigma(t) \quad (3)$$

where $K_m(t)$ and $\sigma(t)$ are the mean and the standard deviation of the null distribution of $K(t)$. The standardized values of the observed $K(t)$ and the 95% simulation envelope were plotted together against the distance, t. Positive values of standardized K-function, $K_{st}(t)$, for a distance indicate clustering (underdispersion) at the scale of the distance, while negative values indicate regularity (overdispersion). Spatial clustering or regularity at the scale of a distance is statistically significant if the value of the observed $K(t)$ for the distance falls outside the 95% simulation envelope in the plot.

doi: 10.1111/j.1349-7006.2009.01437.x

Results

MSI Screening. B-LBL-derived DNA samples ($n = 16$) were investigated at each of the 150 microsatellite markers positioned to span the entirety of MMU3–6. These chromosomes were selected on the basis of displaying the closest resemblance to MMU3 in terms of total estimated length (maximum variance 10 Mb), as determined via data retrieved from the MGB.[27] Our genome-wide screening using microsatellite markers revealed three variant representations of MSI in lymphoma-derived DNA: insertions, deletions, and insertion/deletions (Fig. 1A). MSI was observed at 2≤ microsatellite loci in lymphoma-derived DNA obtained from 15 (93.7%) SL/Kh mice; however, no MSI was observed in healthy splenic DNA derived from SL/Kh mice. Thus, the identified mutations in SL/Kh lymphoma-derived DNA are considered to be tumor-specific and not random background instability.[33] Additionally, BM-derived DNA obtained from NFS/N and NFS.SL/Kh–*Bomb1* mice screened in parallel with SL/Kh specimens were consistently negative for MSI at all examined loci (Fig. 1B). In total, 34 (22.6%) of the investigated markers demonstrated discernible MSI in SL/Kh lymphoma-derived DNA, while all others (77.3%) were negative for gross genomic instability. To ascertain the results obtained from our preliminary MSI screening using 3% agarose gel electrophoresis, we retested the samples originally screened as MSI positive via capillary electrophoresis (Fig. 1C).

Table 1. MSI-positive markers

Marker†	MMU‡	Marker position (cM§)	Repeat unit	Mutation phenotype¶	No. MSI-positive samples (%)
D3Mit139	3	43.6	GT	Insertion	9 (56.2)
D3Mit77	3	49.7	GT	Deletion	9 (56.2)
D3Mit343	3	52.5	CA	Insertion	9 (56.2)
D3Mit300	3	55.0	GT	Insertion	8 (50.0)
D3Mit80	3	58.8	CA	Deletion	9 (56.2)
D3Mit319	3	61.8	CA	Insertion/ Deletion	8 (50.0)
D3Mit290	3	64.1	CA	Insertion	1 (7.6)
D3Mit256	3	66.2	GT	Deletion	9 (56.2)
D3Mit291	3	66.2	GT	Deletion	9 (56.2)
D3Mit351	3	68.5	CA	Deletion	9 (56.2)
D3Mit258	3	70.3	CA	Insertion	10 (62.5)
D3Mit113	3	72.0	GT	Insertion	1 (7.6)
D3Mit321	3	76.2	CA	Insertion	9 (56.2)
D3Mit45	3	78.5	GT	Deletion	9 (56.2)
D3Mit352	3	83.5	CA	Deletion	9 (56.2)
D3Mit129	3	84.9	CA	Insertion	9 (56.2)
D3Mit163	3	87.6	GT	Deletion	8 (50.0)
D4Mit64	4	1.9	GT	Insertion	5 (31.2)
D4Mit317	4	2.5	CAAA	Deletion	5 (31.2)
D4Mit233	4	75.5	GT	Insertion	7 (43.7)
D4Mit180	4	81.0	CA	Insertion	9 (56.2)
D4Mit254	4	82.5	GT	Deletion	9 (56.2)
D5Mit331	5	3.0	CA	Deletion	7 (43.7)
D5Mit386	5	14.0	CA	Deletion	7 (43.7)
D5Mit421	5	21.0	CA	Insertion	7 (43.7)
D5Mit77	5	24.0	CA	Deletion	7 (43.7)
D5Mit132	5	29.0	GT	Insertion	7 (43.7)
D3Mit239	5	58.0	GT	Insertion	9 (56.2)
D6Mit275	6	25.5	GT	Insertion	10 (62.5)
D6Mit95	6	30.0	CA	Insertion	10 (62.5)
D6Mit208	6	32.5	GT	Insertion	10 (62.5)
D6Mit249	6	39.0	GT	Insertion	10 (62.5)
D6Mit230	6	43.0	GT	Deletion	10 (62.5)
D6Mit134	6	57.5	GT	Insertion	6 (37.5)

†DNA segment, chromosome no., name of laboratory that discovered the segment (Massachusetts Institute of Technology; MIT), and serial number assigned by order of discovery on each chromosome by the discovering laboratory; ‡mouse chromosome number where marker is located; §marker position on chromosome designated in cM, centimorgans (cM); ¶type of mutation identified at marker: insertion, deletion, or insertion/deletion. MMU, mus musculus chromosome; MSI, microsatellite instability.

Chromosomal MSI distribution and incidence. Our preliminary results showed that MMU3 seemingly harbors a higher overall incidence of MSI, thus we investigated whether the *Bomb1* region is intrinsically more unstable than other autosomal regions of the lymphoma genome. To this end, a framework map was constructed for each of the mouse chromosomes examined, illustrating the approximate chromosomal positions and incidence of MSI-positive samples per marker. The patterns of MSI distribution within the B-LBL genome are given for MMU3-6 in Figure 2(A–D).

MSI incidence per marker was obtained by dividing the number of MSI-positive samples by the total number of B-LBL samples tested ($n = 16$). Similarly, mean MSI ratios were determined for each chromosome by calculating the combined average incidence of MSI for each marker tested. The overall MSI ratios for MMU3–6 were 0.213 (mean), 0.07, 0.066, and 0.097, respectively. While relatively comparable results were obtained for MMU4, MMU5, and MMU6, significantly higher incidences of MSI ($P = 0.031$) were confirmed on MMU3, which harbors the *Bomb1* locus (Fig. 2E). When the same calculations were performed neglecting the data obtained from the *Bomb1* markers, the overall incidence of MSI on MMU3 (0.116) resembled that of the remaining chromosomes tested ($P = 0.754$). Percentages of MSI-positive B-LBL samples per unstable marker, along with marker position and repeat units, are provided in Table 1. Notably, each of the markers presenting with gross instability displayed total consistency with regard to the type of MSI (insertion, deletion, or insertion/deletion) observed among samples.

Point pattern of MSI-susceptible loci along the chromosomes. The *K*-function analysis was performed collectively for the four chromosomes examined. The observed point pattern is comprised of 32 microsatellite loci with high MSI incidence (more than 0.3) distributed over the four chromosomes. The standardized version of the observed *K*-function and the corresponding 95% simulation envelope are shown in Figure 3(A). The observed *K*-function lies above the 95% simulation envelope at distances from 4 to 50 cM, indicating significant clustering of the MSI-susceptible loci over the range of scales. Spatial clustering is most marked at the scale of 18–20 cM (Fig. 3A), where the extent of deviation from the null distribution is most prominent ($P < 0.002$).

To identify the chromosomal locations of the clustering of MSI-susceptible loci, we calculated local frequencies of loci relative to that of the microsatellite markers for each segment of the scale at which clustering was most marked (=19 cM) and mapped them over the chromosomes. In Figure 3(B), for each genomic position, a value is plotted that indicates the observed count of MSI-susceptible loci within 19 cM of the position divided by the count of the actually examined microsatellite markers within the same segment. To correct the edge effect, for the region beyond the terminus of a chromosome, the ratio of frequency of MSI-susceptible loci to microsatellite markers was assumed to be constantly equal to the expected ratio (=32/150). The shaded areas cover the genomic positions that display a ratio of frequencies above the expected ratio, which denotes clustering of MSI-susceptible loci. A region demonstrating the most extensive clustering is clearly recognized toward the telomere of MMU3.

Discussion

The results obtained from our genome-wide screening and spatial point pattern analysis clearly indicate the presence of MSI-susceptible loci forming clusters across the lymphoma genome. While the *Bomb1* locus is the most outstanding example of the clustering of MSI-susceptible loci, similar patterns of cluster distribution, albeit on a smaller scale, were duly noted on the other chromosomes we investigated as well.

The preliminary results we obtained advocate the theory that the *Bomb1* locus harbors a greater number of MSI-susceptible loci over other autosomal regions of the genome; however, the full range of instability in the B-LBL genome will not be apparent until more samples are dissected at the fine-scale level. Similarly, while the strength of this study lies in the large number of markers tested and meticulous screening methods, it is conceivable that we might have improved our chances of detecting MSI in the *Bomb1* locus in greater quantities owing to the greater number of markers being tested on MMU3. This was due to the increased availability of markers on MMU3 from the original QTL analyses performed on *Bomb1*.

One of the striking features associated with this study was the uniformity of MSI manifestation obtained at each of the MSI presenting markers. Numerous studies have shown that the healthy genome of inbred strains display apparent polymorphisms in genomic copy number[34–36] and other genetic differences;[37] however, to our knowledge, this is the first study to extensively document the uniformity of post-tumorigenic mutations in the cancer genome of a well-maintained inbred strain of mice.

The rapidly expanding repertoire of MSI-associated malignancies warrants further investigation into the individual characteristics of MSI distribution in diverse cancer genomes. This bears significant value to researchers and clinicians alike, for the presence or absence of the MSI phenotype in a defined subset of cancers has monumental impact on the clinical prognosis and treatment of patients.[38–40] Additionally, because MSI investigations on humans have been incremental rather than groundbreaking, similar studies encompassing a variety of laboratory animals and strains could aide in deciphering the code for the biological mechanism governing MSI manifestation in mammalian malignant neoplasms. The results of this and similar studies characterizing MSI in a broad spectrum of cancers could lead to the advent of disease-specific MSI panels, and further holds the possibility of uncovering the existence of heritable patterns of post-tumorigenic genomic instability in mammals.

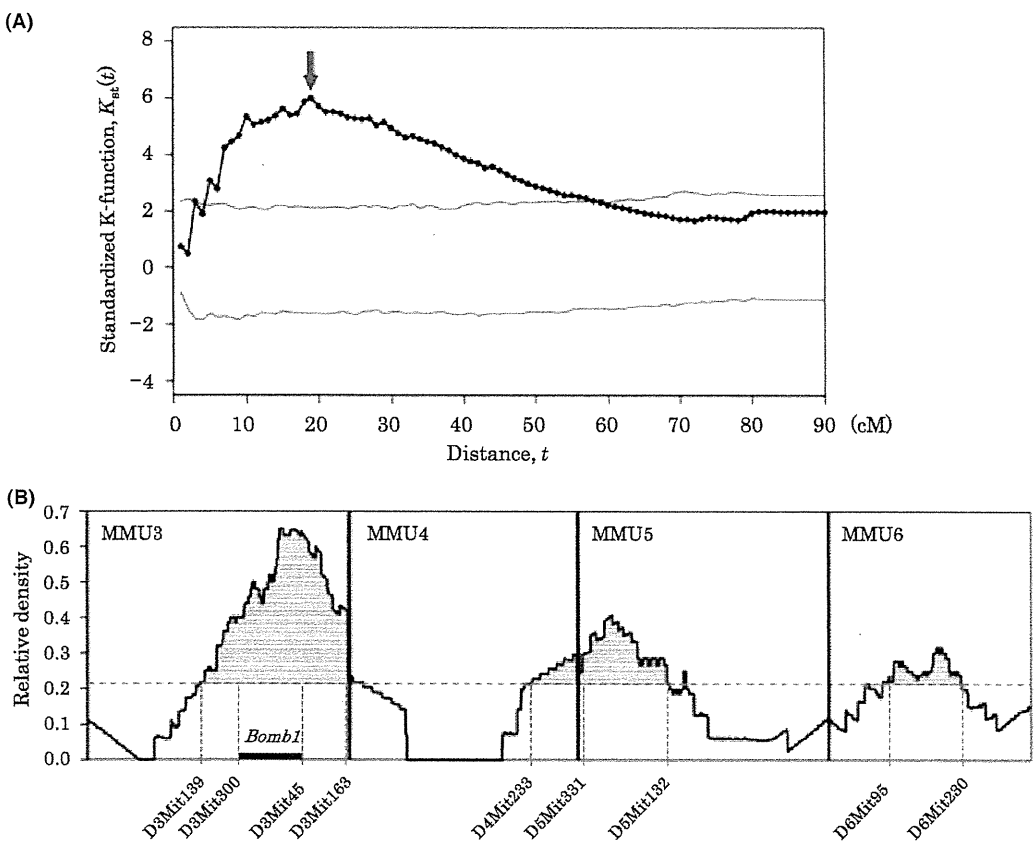

Fig. 3. Spatial point pattern analysis. Point pattern analysis for the distribution of microsatellite instability (MSI)-susceptible loci along the chromosomes. (A) Plot of standardized *K*-function for observed data (dark line) and 95% simulation envelope (gray lines). Statistical significance of the clustering of MSI-susceptible loci is shown at the 0.05 level for distance, *t* (cM), where portions of the dark line stray above the upper gray line. Arrow indicates the point at which the observed *K*-function deviates maximally from the null distribution for equal probabilities. (B) Chromosomal map of local density of MSI-susceptible loci in the scale showing most significant clustering (=19 cM). *Y*-axis indicates the observed count of MSI-susceptible loci within 19 cM of each chromosomal position divided by the count of the actually examined microsatellite markers within the same segment. Dashed line denotes overall density (=32/150). Shaded areas represent genomic positions displaying a ratio of frequencies above the expected ratio (clustering). A region demonstrating the most extensive clustering is clearly recognized in the vicinity of the *Bomb1* locus on mus musculus chromosome (MMU)3. cM, centimorgans.

doi: 10.1111/j.1349-7006.2009.01437.x

Acknowledgments

This work was supported by a Grant-in-Aid for Cancer Research from the Ministry of Education, Culture, Sports, Science, and Technology, Japan, and a Grant for Strategic Research on Cancer from the Ministry of Health, Labor, and Welfare, Japan. Additionally, we are grateful for the generous financial support provided by the Kyoto Shimizu Immunology Foundation. Lastly, we wish to thank Mr. Chihiro Kawai, Ms. Yukiko Imai, Mr. Haruya Takeuchi and Ms Hiroko Saito at the Department of Forensic Medicine and Molecular Pathology, Kyoto University Graduate School of Medicine for their technical assistance.

References

1 Soslow RA, Baergen RN, Warnke RA. B-Lineage lymphoblastic lymphoma is a clinicopathologic entity distinct from other histologically similar aggressive lymphomas with blastic morphology. *Cancer* 1999; **85**: 2648–54.
2 Cheng A-L, Su I-J, Tien H-F, Wang C-C, Chen Y-C, Wang C-H. Characteristic clinicopathologic features of adult B-cell lymphoblastic lymphoma with special emphasis on differential diagnosis with an atypical form probably of blastic lymphocytic lymphoma of intermediate differentiation origin. *Cancer* 1994; **73**: 706–10.
3 Sander CA, Jaffe ES, Gebhardt FC, Yano T, Medeiros LJ. Mediastinal lymphoblastic lymphoma with an immature B-cell immunophenotype. *Am J Surg Pathol* 1992; **16**: 300–5.
4 Link MP, Roper M, Dorfman RF, Crist WM, Cooper MD, Levy R. Cutaneous lymphoblastic lymphoma with pre-B markers. *Blood* 1983; **61**: 838–41.
5 Pattengale PK, Frith CH. Immunomorphologic classification of spontaneous lymphoid cell neoplasms occurring in female BALB/c mice. *J Natl Cancer Inst* 1983; **70**: 169–79.
6 Hiai H, Kaneshima H, Nakamura H, Oguro BY, Moriwaki K, Nishizuka Y. Unusually early and high rate of spontaneous occurrence of nonthymic leukemias in SL/Kh mice, a subline of SL strain. *Jpn J Cancer Res* 1982; **73**: 603–13.
7 Hiai H, Tsuruyama T, Yamada Y. Pre-B lymphomas in SL/Kh mice: a multifactorial disease model. *Cancer Sci* 2003; **94**: 847–50.
8 Shimada MO, Yamada Y, Nakakuki Y *et al.* SL/Kh strain mice: a novel animal model of pre-B lymphomas. *Leuk Res* 1993; **17**: 573–8.
9 Okamoto K, Yamada Y, Shimada MO, Nakakuki Y, Nomura H, Hiai H. Abnormal bone marrow B-cell differentiation in pre-B lymphoma prone SL/Kh mice. *Cancer Res* 1994; **54**: 399–402.
10 Lu LM, Shimada M, Higashi S, Zeng ZZ, Hiai H. Bone marrow pre-B-1 (*Bomb1*): a quantitative trait locus inducing bone marrow pre-B 1 cell expansion in lymphoma-prone SL/Kh mice. *Cancer Res* 1999; **59**: 2593–5.
11 Hiratsuka T, Tsuruyama T, Kaszynski R *et al.* Bone marrow pre-B expansion by SL/Kh-Bomb1 locus: not sufficient for lymphomagenesis. *Leuk Res* 2008; **32**: 309–14.
12 Aaltonen LA, Peltomaki P, Leach FS *et al.* Clues to the pathogenesis of familial colorectal cancer. *Science* 1993; **260**: 812–6.
13 Thibodeau SN, Bren G, Schaid D. Microsatellite instability in cancer of the proximal colon. *Science* 1993; **260**: 816–9.
14 Eshleman JR, Markowitz SD. Mismatch repair defects in human carcinogenesis. *Hum Mol Genet* 1996; **5**: 1489–94.
15 Ionov Y, Peinado MA, Malkhosyan S, Shibata D, Perucho M. Ubiquitous somatic mutations in simple repeated sequences reveal a new mechanism for colonic carcinogenesis. *Nature* 1993; **363**: 558–61.
16 Moslein G, Tester DJ, Lindor NM *et al.* Microsatellite instability and mutation analysis of hMSH2 and hMLH1 in patients with sporadic, familial and hereditary colorectal cancer. *Human Mol Genet* 1996; **5**: 1245–52.
17 Burks RT, Kessis TD, Cho KR, Hedrick L. Microsatellite instability in endometrial carcinoma. *Oncogene* 1994; **9**: 1163–6.
18 Mironov NM, Aguelon MA-M, Potapova GI *et al.* Alteration of (CA)n DNA repeats and tumor suppressor genes in human gastric cancer. *Cancer Res* 1994; **54**: 41–4.
19 Shridhar V, Siegfried J, Hunt J, Alonso M, Smith DI. Genetic instability of microsatellite sequences in many non-small cell lung carcinomas. *Cancer Res* 1994; **54**: 2084–7.
20 Uchida T, Wada C, Wang C, Egawa S, Ohtani H, Koshiba K. Genomic instability of microsatellite repeats and mutations of H-, K-, and N-ras and p53 genes in renal cell carcinoma. *Cancer Res* 1994; **54**: 3682–5.
21 Yee JC, Roodi N, Verrier C, Parl FF. Microsatellite instability and loss of heterozygosity in breast cancer. *Cancer Res* 1994; **54**: 1641–4.
22 Niv E, Bomstein Y, Bernheim J, Lishner M. Microsatellite instability in gastric MALT lymphoma. *Mod Pathol* 2004; **17**: 1407–13.
23 Han HJ, Yanagisawa A, Kato Y, Park JG, Nakamura Y. Genetic instability in pancreatic cancer and poorly differentiated type of gastric cancer. *Cancer Res* 1993; **53**: 5087–9.
24 Gonzalez-Zulueta M, Ruppert JM, Tokino K *et al.* Microsatellite instability in bladder cancer. *Cancer Res* 1993; **53**: 5620–3.
25 Gurin CC, Federici MG, Kang L, Boyd J. Causes and consequences of microsatellite instability in endometrial carcinoma. *Cancer Res* 1999; **59**: 462–6.
26 Hanford MG, Rushton BC, Gowen LC, Farber RA. Microsatellite mutation rates in cancer cell lines deficient or proficient in mismatch repair. *Oncogene* 1998; **16**: 2389–93.
27 Bult CJ, Eppig JT, Kadin JA *et al.* The Mouse Genome Database (MGD): mouse biology and model systems. *Nucleic Acids Res* 2008; **36**: D724–8. [Cited 1 Nov 2008.] Available from URL: http://www.informatics.jax.org/mgihome/other/mouse_facts1.shtml
28 Chattopadhyay SK, Lowy DR, Teich NM, Levine AS, Rowe WP. Evidence that the AKR murine leukemia virus genome is complete in DNA of the high-virus AKR mouse and incomplete in the DNA of the "virus-negative" NIH mouse. *Proc Natl Acad Sci USA* 1974; **71**: 167–71.
29 Fredrickson TN, Morse HC III, Rowe WP. Spontaneous tumors of NFS mice congenic for ecotropic murine leukemia virus induction loci. *J Natl Cancer Inst* 1984; **73**: 521–4.
30 Kraft CE, Warren DR. Development of spatial pattern in large woody debris and debris dams in streams. *Geomorphology* 2003; **51**: 127–39.
31 Ripley BD. The second-order analysis of stationary point processes. *J Appl Probab* 1976; **13**: 255–66.
32 Ersbøll AK, Ersbøll BK. Simulation of the K-function in the analysis of spatial clustering for non-randomly distributed locations – exemplified by bovine virus diarrhoea virus (BVDV) infection in Denmark. *Prev Vet Med* 2009; **91**: 64–71.
33 Weber JL, Wong C. Mutation of human short tandem repeats. *Hum Mol Genet* 1993; **2**: 1123–8.
34 Watkins-Chow DE, Pavan WJ. Genomic copy number and expression variation within the C57BL/6J inbred mouse strain. *Genome Res* 2008; **18**: 60–6.
35 Li J, Jiang T, Mao J-H *et al.* Genomic segmental polymorphisms in inbred mouse strains. *Nat Genet* 2004; **36**: 952–4.
36 Snijders AM, Nowak NJ, Huey B *et al.* Mapping segmental and sequence variations among laboratory mice using BAC array CGH. *Genome Res* 2005; **15**: 302–11.
37 Specht CG, Schoepfer R. Deletion of the alpha-synuclein locus in a subpopulation of C57BL/6J inbred mice. *BMC Neurosci* 2001; **2**: 11.
38 Sankila R, Aaltonen LA, Jarvinen HJ, Mecklin JP. Better survival rates in patients with MLH1-associated hereditary colorectal cancer. *Gastroenterology* 1996; **110**: 682–7.
39 Kohonen-Corish MR, Daniel JJ, Chan C *et al.* Low microsatellite instability is associated with poor prognosis in stage C colon cancer. *J Clin Oncol* 2005; **23**: 2318–24.
40 Wright CM, Dent OF, Newland RC *et al.* Low level microsatellite instability may be associated with reduced cancer specific survival in sporadic stage C colorectal carcinoma. *Gut* 2005; **54**: 103–8.

Supporting Information

Additional Supporting Information may be found in the online version of this article:

Data S1. Markers examined in this study are as follows (values in parentheses denote chromosomal position in cM).

Please note: Wiley-Blackwell are not responsible for the content or functionality of any supporting materials supplied by the authors. Any queries (other than missing material) should be directed to the corresponding author for the article.

JLB

Article

Dual retrovirus integration tagging: identification of new signaling molecules *Fiz1* and *Hipk2* that are involved in the IL-7 signaling pathway in B lymphoblastic lymphomas

Tatsuaki Tsuruyama,[*,1] *Yukiko Imai,*[*] *Haruya Takeuchi,*[*] *Takuya Hiratsuka,*[†] *Yasuhiro Maruyama,*[‡] *Kazuya Kanaya,*[‡] *Richard Kaszynski,*[*] *Guang Jin,*[§] *Tomoko Okuno,*[*] *Munetaka Ozeki,*[*] *Takuro Nakamura,*[§] *Tetsuya Takakuwa,*[‡] *Toshiaki Manabe,*[†] *Keiji Tamaki,*[*] *and Hiroshi Hiai*[‖]

[*]Department of Forensic Medicine and Molecular Pathology, [†]Department of Diagnostic Pathology, and [‡]Department of Human Health Science, Graduate School of Medicine, Kyoto University, Kyoto, Japan; [§]Laboratory of Carcinogenesis, Cancer Institute, Tokyo, Japan; and [‖]Shiga Medical Center Research Institute, Shiga, Japan

RECEIVED NOVEMBER 9, 2009; REVISED FEBRUARY 11, 2010; ACCEPTED MARCH 5, 2010. DOI: 10.1189/jlb.1109748

ABSTRACT

IL-7R, FLT3, and CD43 are surface antigens expressed during the transition from pro-B to pre-B cells in BM. To understand interactions between their signaling pathways, we analyzed spontaneous mouse B-LBLs with dual MLV integration into *Stat5a* and *Fiz1* or *Stat5a* and *Hipk2*. MLV integration resulted in up-regulation of these genes in lymphoma cells compared with normal pro-B cells from the BM. In lymphomas with both integrations into *Stat5a* and *Fiz1*, increases in phosphorylated STAT5A and expression of c-Myc, a target gene of STAT5A, were observed following stimulation of the FLT3. Clones with the dual integrations grew faster in IL-7 and FLT3L-supplemented medium than clones with *Stat5a* integration alone. On the other hand, in lymphomas with integrations into *Stat5a* and *Hipk2*, increases in phosphorylated STAT5A and expression of c-Myc were observed following cross-linking of CD43. In conclusion, FLT3 and CD43 signaling pathways involve STAT5A via *Fiz1* and *Hipk2* in B-LBLs. Identification of the dual MLV integration sites in B-LBLs, therefore, will provide an excellent tool for identification of the signaling pathways in B-LBLs. *J. Leukoc. Biol.* 88: 107–116; 2010.

Introduction

Retroviral insertional mutagenesis in several inbred strains of mice induces a high incidence of myeloid leukemia and B and T cell lymphomas, as well as other types of tumors [1]. The retroviral integration sites in these tumors thus provide powerful tools for the identification of novel oncogenes and tumor-related genes [2]. The inbred strain of mice SL/Kh develops lymphoma spontaneously as a result of genetically acquired MLV integration [3, 4]. More than 90% of these mice develop $B220^+$ $BP\text{-}1^+$ $CD43^+$ $CD24^+$ $sIgM^-$ B-LBLs spontaneously by 6 months of age [5]. As development of spontaneous B-LBLs is rare in most other mice, the SL/Kh strain is an important model for studying the pathogenesis of B-LBLs. By analyzing (SL/Kh×NFS/N) × NFS/N F2, we have mapped a highly significant quantitative trait locus, named Bomb1, on the distal segment of mouse chromosome 3, which is responsible for pre-B expansion [6]. NFS/N is an inbred mouse strain without an endogenous, ecotropic MLV genome and with low spontaneous lymphoma incidence [7]. We generated a congenic strain, NFS/N.SL/Kh-Bomb1 mice, in which the Bomb1 locus is replaced by the identical locus in the SL/Kh mice genome. We observed that the congenic mice showed pre-B cell expansion after 4 months of the birth and demonstrated that the Bomb1 locus is crucial for the pre-B expansion [8]. Such spontaneous lymphoma strains have been used as a tool to search for novel oncogenes by identification of common integration sites of MLV [1, 2]. Reintegration of endogenous MLV genomes into the cancer-related genes *Stat5a* [9] and *c-myc* [10] induced these lymphomas. In this study, we show that these mice are also a useful model for investigation of oncogene pathway interactions by analysis of lymphomas with dually integrated, clonal MLVs. Wu et al. [11] reported that MLV integration favors transcriptionally active genes. Therefore, when lymphoma cells have more than one clonally integrated MLV ge-

Abbreviations: B-LBL=B-lymphoblastic lymphoma, BM=bone marrow, Bomb1=bone marrow pre-B-1, D_H-J_H=Ig heavy chain diversity-joining, *Emv11*=endogenous ecotropic MuLV11, *Fiz1*= fms-like tyrosine kinase 3-interacting zinc finger protein 1, FLT3L=fms-like tyrosine kinase 3 ligand, *Hipk2*=CD43-interacting homeodomain-interacting protein kinase 2, *IgH*=Ig heavy chain, *IgL*=Ig light chain, ITD=internal tandem duplication, MLV=murine leukemia retrovirus, sIgM=surface IgM

1. Correspondence: Department of Forensic Medicine and Molecular Pathology, Graduate School of Medicine, Yoshida-konoe-cho, Sakyo-ku, Kyoto 606-8501, Japan. E-mail: tsuruyam@kuhp.kyoto-u.ac.jp

nome, the host genes are likely to be commonly active, and their interaction can be observed in the host cells. We reported previously that one of the common integration sites of MLV in SL/Kh B-LBLs is *Stat5a*, whose constitutive activation is responsible for pre-B cell lymphomagenesis in vivo and in vitro [9]. Activated STAT5A forms a dimer and influences transcriptional activity of other genes by binding to the γ-activated site element in the promoter of target antiapoptotic genes, such as *c-myc*, *pim-1*, *bcl-xL*, and *cyclin D1* [12–15]. STAT5A is recruited in the IL-7R pathway that operates selectively during the precursor stage of the pro- to pre-B cell transition in BM, as well as in T cells [15, 16].

In the current study, we show two novel types of signaling pathways that were activated by MLV integration. We also identify a novel pathway involved in cellular signaling transmission by analysis of the signaling pathways. We examined the *c-myc* expression via the STAT5A phosphorylation [9]. STAT5 is essential for early B cell development but not for B cell maturation and function [17]. This IL-7R pathway is key in pro-B cell development and is known to regulate IgH recombination and B cell precursor expansion [18, 19]. STAT5 and IL-7 signaling control cell survival and the developmental ordering of Ig gene rearrangements by suppressing premature Igκ recombination in pro-B cells [20]. Thus, the occurrence of B-LBLs in SL/Kh mice caused by *Stat5a* integration is a promising model for investigation of one of the signaling pathways in early B lymphocytes [5]. The development stage of B cells was according to Hardy's standard classification of murine B cell lineage [21]. In the current study, we identified novel integration sites in SL/Kh B-LBLs including *Fiz1* and *Hipk2*. *Fiz1* encodes a novel zinc finger protein with C_2H_2-type zinc fingers that interacts with the receptor tyrosine kinase FLT3 [22], a surface antigen of pro- to pre-B cells. On the other hand, *Hipk2* encodes a member of a novel family of serine/threonine kinases [23] that interacts with the cytoplasmic domain of CD43, which is expressed on most hematopoietic cells, including pro- to pre-B cells. Although the host genes activated by MLV integration were different, the type of lymphoma was consistently B-LBLs. This suggests that cross-talk may be involved in the intracellular pathways activated by the MLV integration. As several clones of cells from SL/Kh B-LBLs had dual *Stat5a* and *Fiz1* or *Stat5a* and *Hipk2* integrations, we studied the cross-talk among signaling molecules in the IL7-R pathway. These data provide novel insights into the pathogenesis of B-LBLs.

MATERIALS AND METHODS

Animals

The origin, endogenous MLVs, and host genetic factors in lymphomagenesis in SL/Kh mice have been reported previously [3–6]. All animal experiments were carried out with approval from the Ethical Committee for Animal Experiments, Kyoto University Graduate School of Medicine (Japan).

Inverse PCR for identification of MLV integration sites

The virus-host junctions of the MLV integration site were amplified with inverse PCR [9]. In brief, genomic DNA (100 ng) from each lymphoma was digested with *Sac*II for 2 h and self-ligated with T4 ligase (Takara Bio, Otsu, Japan) at 14°C overnight. PCR amplification was carried out in three steps in a thermal cycler (Takara Bio) under the following conditions: initial denaturation (1 min at 95°C); then 10 cycles (30 s at 94°C, 40 s at 62°C, and 4 min at 68°C; step 1); then 20 cycles (30 s at 94°C, 40 s at 62°C, and 4 min plus extension of 20 s in one cycle at 68°C; step 2); and finally, elongation (10 min at 72°C). In some cases, nested PCR was added to the above reaction. The primers for inverse PCR were located within the MLV genomes. Their

TABLE 1 *Phenotypic Features of Lymphoma*

			IgH								
ID	Sex	Age	D_HJ_H	V_HD_H	IgL	CD43	IL-7R	CD24	V_{preb}	λ5	Integration site
1	f	6	c	n.d.	g	+	+	+	+	–	*Stat5a*
2	m	7	c	n.d.	g	+	+	+	+	–	*Stat5a*
3	f	4	c	n.d.	g	+	+	+	+	–	*Stat5a*
4	m	6	c	c	g	+	+	+	+	–	*Stat5a*
5	f	7	c	c	g	+	+	+	+	–	*Stat5a*
6	f	6	c	c	g	+	+	+	+	–	*Stat5a*
7	m	7	c	n.d.	g	+	+	+	+	–	*Fiz1* + *Stat5a*
8	f	6	c	n.d.	g	+	+	+	+	–	*Fiz1* + *Stat5a*
9	f	10	c	n.d.	g	+	+	+	+	–	*Fiz1* + *Stat5a*
10	m	5	c	n.d.	g	+	+	+	+	–	*Fiz1* + *Stat5a*
11	m	4	c	c	g	+	+	+	+	–	*Fiz1* + *Stat5a*
12	f	9	c	c	g	+	+	+	+	+	*Fiz1*
13	m	6	c	c	g	+	+	+	+	+	*Fiz1*
14	f	7	c	c	g	+	+	+	+	+	*Fiz1*
15	f	5	c	c	g	+	+	+	+	+	*Hipk2*
16	m	8	c	n.d.	g	+	+	+	+	–	*Hipk2*
17	f	4	c	n.d.	g	+	+	+	+	–	*Hipk2* + *Stat5a*
18	m	5	c	c	g	+	+	+	+	–	*Hipk2* + *Stat5a*
19	f	6	c	c	g	+	+	+	+	–	*Hipk2* + *Stat5a*
20	m	7	c	c	g	+	+	+	+	–	*Hipk2* + *Stat5a*
21	m	3	c	c	g	+	+	+	+	–	*Hipk2* + *Stat5a*

f, Female; m, male; c, completed (D_HJ_H); n.d., not detected (V_HD_H); g, germ line (IgL); V_HD_H, variable of IgH.